Alteration rate of medieval potash-lime silicate glass as a function of pH and temperature: A low pH-dependent dissolution

Loryelle Sessegolo, Aurélie Verney-Carron, Patrick Ausset, Sophie Nowak, Sylvain Triquet, Mandana Saheb, Anne Chabas

Alteration rate of medieval potash-lime silicate glass as a function of pH and temperature: a low pH-dependent dissolution

Loryelle Sessegolo[1*], Aurélie Verney-Carron[1], Patrick Ausset[1], Sophie Nowak[2], Sylvain Triquet[1], Mandana Saheb[1], Anne Chabas[1]

[1]LISA, UMR CNRS 7583, Université Paris-Est-Créteil, Université de Paris, Institut Pierre Simon Laplace (IPSL), Créteil, France
[2]Plateforme Rayons X, UFR de Chimie, Université Paris Diderot, Paris, France

∗ Corresponding author at: Laboratoire Interuniversitaire des systèmes atmosphériques, Université Paris-Est Créteil, 61 avenue du Général de Gaulle, 94000 Créteil, France.
E-mail address: loryelle.sessegolo@gmail.com

Abstract

Potash lime silicate glasses were extensively used during the Middle Ages as components of stained glass windows. Their external faces have been subjected to alteration in the atmospheric medium for centuries, leading to the development of thick alteration layers on the surfaces. This alteration is mainly caused by water in liquid (rainfall) or gaseous (vapor) form. In order to implement geochemical models simulating the long-term behavior of these glasses by coupling the different atmospheric factors, it is necessary to study mechanisms and kinetics of alteration induced by these different hygroscopic situations (rainfall and relative humidity). The aim of this study is here to evaluate the impact of liquid water on stained glass windows and especially to determine alteration rate laws of dissolution and interdiffusion as a function of pH and temperature. For that, a medieval model glass was altered in aqueous solution in batch experiments at different pH values (from 2 to 11), temperatures (from 5 to 70°C) and saturation states of the solution. From the elemental concentrations in solution, the release rate of elements was calculated and the pH- and T-dependencies were determined. The dissolution and interdiffusion rate laws can now be used to simulate the alteration of a medieval glass submitted to a rainfall event. Moreover, this study highlights that the Si-K-Ca medieval glass presents a very low pH-dependency at alkaline pH, which can be explained by its composition.

1) Introduction

Many stained glass windows that currently decorate religious buildings were made during the medieval period, especially during the XII-XIVth c. At this time, glasses were composed of a high content of modifier cations, mainly potassium and calcium (generally between 10 and 20 wt.% of K_2O and CaO each) and a low silica content around 50 wt.%, (Carmona et al., 2006;

Garcia Vallès and Vendrell Saz, 2002; Lombardo et al., 2010; Schalm et al., 2007; Sterpenich and Libourel, 2006, 2001). Because of this composition, these glasses are considered to be low durable as modifiers induce the breaking of Si-O-Si Bridging Oxygen (called "BO") to form Si-O-M Non-Bridging Oxygen (with M a cation; called "NBO"). The glass is thus more highly vulnerable to chemical attacks caused by liquid water (saturated medium) as well as water vapor (unsaturated medium) (De Ferri et al., 2014; Melcher and Schreiner, 2006; Woisetschläger et al., 2000). Therefore, stained glass windows exposed for 6 or 7 centuries in atmosphere have developed thick alteration layers up to around 200 µm and different kinds of alteration morphology (Lombardo et al., 2010; Sterpenich and Libourel, 2001). Some of them are covered by a continuous alteration layer (Lombardo et al., 2010; Sterpenich and Libourel, 2001). Others present craters or pits of alteration as well as a fresh surface still observable between each pit (Lombardo et al., 2010; Sterpenich and Libourel, 2001). The alteration layers are often laminated (Lombardo et al., 2013; Schalm and Anaf, 2016).

Generally, dissolution of silicate minerals and glass is driven by water molecules hydrolyzing the different O-bonds (Advocat et al., 1989, 1990a; Casey et al., 1990; Crovisier et al., 1985, 1987). The preferential leaching of alkalis, and sometimes alkaline-earth elements, called interdiffusion, corresponds to an ion exchange between hydrogenated species of the water and modifier cations of the glass (Doremus, 1975; Guy and Schott, 1989; Hellmann, 1997; Houser, C. A. et al., 1980; Lanford et al., 1979; Maurer et al., 1985; Petit et al., 1990; Wassick et al., 1983). This leads to the formation of a hydrated and dealkalinized layer on glass surface, (Doremus, 1975; Petit et al., 1990). This layer can then be reorganized by Si condensation reactions, forming the so-called "gel" layer (Gin et al., 2015, 2018; Valle et al., 2010; Verney-Carron et al., 2017). Verney-Carron et al. (2017) have shown that interdiffusion and hydrolysis / condensation reactions are responsible for the formation of the alteration layer for stained glass windows experimentally altered by rain water.

Repeated rainfall events can lead to a subsequent alteration. This kind of alteration is expected to depend on temperature, flowrate, pH and composition of rainwater. Temperature is variable in the atmosphere. It can be negative during winter and high (until 50°C) in summer at the surface of stained glass canopies. The pH and composition of the rain can also evolve with time and as a function of atmospheric conditions. For example, rains have a current pH between 5.5 and 6.5 (Singh et al., 2016) but in the past, they were more acidic, especially during the 19 and 20^{th} centuries, when SO_2 concentrations in the atmosphere were high (sulfuric acid formation) (Menz and Seip, 2004). Besides, in case of a weak rainfall event or in presence of a condensation film at the surface, the S/V ratio (reactive surface/volume of solution) can be very high and pH can rapidly increase. In the prospect of developing a geochemical model of the alteration of stained glass windows in the atmosphere, it is essential to determine the interdiffusion and dissolution rates of the medieval Si-K-Ca glass as a function of pH, temperature and saturation of the altering solution.

Far from saturation, the dissolution of mineral and glass occurs at the initial dissolution rate r_0. This rate is strongly dependent on the composition of the glass (Chen and Brantley, 1998; Hamilton et al., 2001). Generally, the pH-dependency of the initial dissolution rate is expressed using an empirical coefficient *n* (Advocat et al., 1990a; Blum and Lasaga, 1991; Gislason and Oelkers, 2003; Guy and Schott, 1989; Inagaki et al., 2013):

$$r_0 = k_0(a_{H+})^n \quad \text{Eq. 1}$$

With r_0 the initial dissolution rate (in g.m².d^{-1}), k_0 the initial rate constant (in g.m².d^{-1}), a_{H+} the protons activity and *n* the coefficient of pH-dependency.

The initial dissolution rate also depends on temperature and follows the Arrhenius law (Eq. 2):

$$r_0 = A \exp\left(\frac{-Ea}{RT}\right) \quad \text{Eq. 2}$$

With *Ea* the activation energy (in J.mol^{-1}), *R* the ideal gas constant (J.mol^{-1}.K^{-1}) and *T* the temperature (in K).

Including the two pH- and T-dependencies, a rate law of the initial dissolution commonly used in literature is the following:

$$r_0 = k_0(a_{H+})^n \exp\left(\frac{-Ea}{RT}\right) \quad \text{Eq. 3}$$

When the concentration of Si in solution increases, a rate drop is commonly observed. The dissolution reaction tends towards an equilibrium and its rate decreases. The evolution of the dissolution rate considering the distance from the equilibrium can be expressed using a classical first order law (Aagaard and Helgeson, 1982; Grambow, 1985):

$$r = k_0(a_{H+})^n \exp\left(\frac{-Ea}{RT}\right)\left(1 - \frac{Q}{K}\right) \quad \text{Eq. 4}$$

With *Q* the activity quotient and *K* an equilibrium constant.

For the interdiffusion process, the leaching of alkalis generally follows a square-root of time-dependent rate law. The second Fick's law can be used to determine the diffusion coefficient D (ion diffusion in a semi-infinite 1D medium) from solution analyses or solid characterization. The interdiffusion rate law can be expressed as a function of T and pH with the same mathematical formalism than dissolution (Chave et al., 2007; Verney-Carron et al., 2010):

$$D = D_0\ (a_{H+})^{n'} \exp\left(\frac{-Ea'}{RT}\right) \quad \text{Eq. 5}$$

With *D* the diffusion coefficient (in m².s^{-1}), D_0 the initial diffusion coefficient (in m².s^{-1}), *n'* the pH-dependency and *Ea'* the activation energy related to this process.

The aim of this study is to determine the parameters (k_0, D_0, *n, n', Ea* and *Ea'*) of the rate laws of dissolution and interdiffusion (Eq. 4 and 5) for the case of medieval Si-K-Ca glass. For that, a

model glass with an average composition of medieval glass was synthetized and altered at pH ranging from 2 to 11, at temperatures between 5 and 70°C and at different reaction progresses.

2) Material and methods

2.1) Model glass

The composition of SG3 model glass used for experiments was defined in order to be representative to that of medieval glasses (Table 1). Oxides contents were calculated from the average composition of 23 medieval glass samples: To2, Ev, Op1, Me, DV, DB, RVF and SVJ (Sterpenich and Libourel, 2001, 2006); Ou2b, Ou4b, Ou5a, Ev1b (Lombardo et al., 2010) and 11 medieval samples (Carmona et al., 2006). SG3 was synthesized at the LDMC (Laboratoire de Développement des Matrices de Conditionnement, CEA, France). Ultrapure silica, oxides and carbonates were molten together for 2 hours at 1400°C in a platinum crucible placed in an electric oven. The melted glass was then poured onto a metallic plate and annealed in a graphite crucible at 550°C. The glass barrels were cut into 2.5 x 2.5 x 0.3 cm^3 coupons and both large sides were polished using diamond grain down to a quarter of micrometer. Some monoliths contained a few bubbles. Those chosen for the experiments were the ones containing no or the less possible visible bubbles on surfaces. The glass density was measured by pycnometry and is 2.59 x 10^3 $kg.m^{-3}$.

2.2) Leaching experiments

2.2.1) Experiments far from equilibrium

Experiments were performed in static conditions. Initial pH of solutions from 2 to 11 were adjusted by additions of ultrapure HNO_3 and NaOH into ultra-pure water. They were free to evolve over time since buffers can accelerate or inhibit the dissolution (Dove and Crerar, 1990; Tournié et al., 2013). For each PTFE bottle, a quarter of the SG3 model glass coupon (4.6 cm^2) was immersed in an initial volume of solution of 200 mL, placed directly at the bottom of the bottle regularly stirred. Initial S/V ratio was 2.3 m^{-1} for each reactor. Solutions were punctually sampled. This induced weak S/V variations that were considered in future calculations. The alteration time varies as a function of the experiments (ranging from 1 to 87 days).

2.2.2) Experiments in Si-enriched solutions

In order to limit the contribution of the dissolution process which is expected to be high at alkaline pH, three alteration experiments were performed in static conditions in solutions initially enriched with silica at initial pH of 8.3 at 20°C and of 9 and 10.5 at 70°C. Initial Si-concentrations were 15 ppm for the experiments at 20°C and 40 ppm for 70°C, respectively. Solutions were prepared by dissolving SiO_2 into a few milliliters of NaOH for 1 h on hot plate. In theory, the Si concentration when solution is in equilibrium with amorphous silica is 49 $mg.L^{-1}$ at 20°C and 118 $mg.L^{-1}$ at 70°C (Gunnarsson and Arnórsson, 2000). Here, the Si concentration rapidly rises in solution and tends toward a plateau (around 50 ppm at 20°C and 110 ppm at 70°C and pH < 10, see Suppl. Mat.).

At 20°C, one reactor was filled with 50 mL of the Si-enriched solution at 15 ppm. The pH was adjusted by addition of HNO_3 to reach 8.3. At 70°C, two reactors were filled with the Si-enriched solution at 40 ppm. The pH of the first reactor was 10.5 (at 70°C) and the pH of the second one was adjusted with HNO_3 to reach 9.0 (at 70°C) (both pH values given here were corrected from the temperature effect with JCHESS software, see below). The alteration time depends on the experiment series.

2.3) Analytical methods

Solution samples were diluted with ultra-pure water and acidified with concentrated HNO_3 (1% v/v). They were then analyzed using Inductively Coupled Plasma – Atomic Emission Spectroscopy (ICP-AES) with a Spectro/AMETEK ARCOS instrument located in a clean-room environment. Solutions were introduced using an autosampler (ASX-520 AutoSampler CETAC) under an ISO-2 laminar flow hood. A pneumatic cross-flow nebulizer was used, mounted with a Scott spray chamber. Blanks and standards (SLRS5 and SLRS6, NRC-CNRC) were analyzed as well as control samples every 10 samples to check for drift over time. SLRS6 standard solution is certified for Al, Ca, Fe, K, Mg, Mn and Na. Regarding Si, solutions were prepared by diluting a standard solution. Uncertainties on Si depend on the concentration. Below 100 ppb, uncertainties are 7% for the 4 and 35°C series, 20% for the 50°C series and 13% for the 20 and 70°C series, which were analyzed during different sessions. For concentrations higher than 200 ppb, uncertainties are lower than 10 % for all temperatures series (for a given temperature, all tested pH were analyzed in the same time). Concerning K, the uncertainties ranged between 2 % and 34% as a function of the series.

After the experiment, sample surfaces were directly observed using a Low Vacuum Scanning Electron Microscopy (SEM) Hitachi TM3030 (15 kV) without preparation. Samples in cross-section were embedded under vacuum (JeolJFC-1100E) using an Epofix® resin and polished using first SiC papers (from P400 to P1200) and then diamond powders down to ¼ µm diamond grain. Samples were coated with palladium by vacuum evaporation. EDS (Energy-Dispersive Spectroscopy) characterizations were carried out using a field emission SEM Jeol

JSM-6301F fitted with an EDS Silicon Drift X-Max 80 mm^2 detector and Aztec Advanced-INCA350 analyzer, Oxford Instruments, at 20 kV.

X-Ray Diffraction (XRD) was performed on a Panalytical Empyrean diffractometer (45 kV and 40 mA Cu tube, filtered radiation, PIXCel multi-channel detector), in Bragg-Brentano configuration θ-θ. The optics used are a 0.04 rad soller slot, a 10 mm mask, and a 1/16° divergence slot. The specimen holder is a 5-axis cradle (x, y, z, chi, phi) allowing an optimized surface adjustment. Measurements were made between 5° and 90°, with a pitch between 0.01° and 0.03° for a pause time ranging from 300 s to 600 s (depending on peak width and intensity).

2.4) Calculation of alteration rates

From concentrations of each element *i* analyzed using ICP-AES, normalized mass losses (NL_i in $g.m^{-2}$) were calculated:

$$NL_i = \frac{[i]}{S/V \times x_i} \quad \text{Eq. 6}$$

With [i] the concentration of the element *i* ($mg.L^{-1}$), S the reactive surface area considered here as the geometric surface area (m^2), V the volume of solution (m^3) and x_i the mass fraction of the element *i*.

2.4.1) Initial dissolution rate (r_0)

Initial dissolution rates r_0 (in $g.m^{-2}.d^{-1}$) were calculated from the release of Si which is the tracer of the glass dissolution:

$$r_0 = \frac{\partial NL_{Si}}{\partial t} \quad \text{Eq. 7}$$

The values of Si concentrations for the initial dissolution rate were considered when the Si release in solution had a linear behavior as a function of time (between 1 hour to a few days depending on the temperature and pH).

2.4.2) Interdiffusion rate

In an acidic medium, the dissolution rate is expected to be low compared to the interdiffusion and this process can be neglected in the release of modifier cations (especially of K and Ca in the case of medieval stained glass windows). The diffusion rate can thus be measured in far from equilibrium batch experiments. For alkaline medium, diffusion rates were deduced from

the experiments performed in initially Si-enriched solutions to limit the dissolution contribution in these pH conditions.

Diffusion coefficient D (in m^2s^{-1}) can be calculated from the second Fick's law:

$$\frac{\partial NL_i}{\partial t^{1/2}} = 2\rho\sqrt{\frac{D}{\pi}} \quad \text{Eq. 8}$$

With NL_i the normalized mass losses of the element *i* (in $g.m^{-2}.s^{-1/2}$), *t* the time (in s) and ρ the glass density (in $g.m^{-3}$).

2.5) Geochemical modeling

Aqueous speciation and mineral saturation states were calculated using JCHESS software developed by Mines ParisTech (van der Lee and De Windt, 2002) and CHESS database. It was also used to recalculate the pH at the temperature of the experiment as it was measured at ambient temperature. For experiments where the pH was not fixed, the pH was not measured at every sampling as it can induce some contaminations. The pH was calculated from solution analyses and compared to measured pH when it was measured.

3) Results

3.1) Evolution of the pH

Simulated and measured pH values are presented in Table 2. At acidic pH (pH 3 at 20°C, 35°C, 50°C and 70°C), the pH does not significantly evolve during the first days before a sudden pH jump higher than 7. In these cases, intermediate pH values were calculated from solution analyses using JCHESS to follow the evolution.

For the initial near-neutral pH (pH ~6 at 4°C, 20°C, 35°C, 50°C and 70°C), the pH rapidly increases during the first days (Table 2). Thus, the pH considered is an average value of the samples used for calculations when Si release in solution was linear over time.

For initial pH of ~10 (for 4°C, 20°C, 35°C, 50°C and 70°C), the pH barely evolved over time (Table 2), therefore rates were associated to the initial pH value.

For experiments in Si-enriched solutions at 20 and 70°C (Table 2, 20°C-Si and 70°C-Si), the first sampling of solution was done after 13 days of experiments due to the high dilution imposed for analyses by the high Si concentration in solution. After this period, the initial pH of 8.3 at 20°C has largely evolved to reach 10.3 and not evolved until 20 days (Table 2). Thus, this is the pH value considered for the dissolution rate. For the experiments at 70°C, the pH evolution was not substantial.

3.2) Dissolution stoichiometry

The evolution of normalized mass losses (NL_i, Eq. 6) as a function of time shows a very clear difference in species behavior according to pH. Interdiffusion and dissolution contributions evolve as a function of this parameter. Figure 1 presents an example of NL_i for samples altered at 50 ± 2°C during 24 h at several pH values under static conditions. Only this figure is shown here although the behavior of glass elements is similar whatever the temperature (see Tables S1 and S2 in Supplementary Material for all the values of concentrations, time and S/V).

At a very acidic pH (2.0 ± 0.1), glass dissolution is non-stoichiometric: modifier cations are released in solution at a higher rate than that of silicon (Fig. 1a). At pH 5.4 and 6.3, the alkaline and alkaline-earth elements are still released at slightly higher rate than silicon (Fig. 1b and c), but at pH 9.8, glass dissolution is congruent (Fig. 1d). Non-stoichiometric dissolution mainly occurs in acidic to neutral medium and then gradually evolves to congruent dissolution, where the hydrolysis of the glassy network is faster than interdiffusion.

In solution initially enriched in silicon, the release of Si decreases and the interdiffusion is the predominant mechanism (Fig. 2).

3.2) pH- and T-dependencies of dissolution

The initial alteration rate (Eq. 3) was measured in the first hours or days, where pH is constant and Si release evolves linearly over time. The Si concentrations used for calculations are lower than 4 ppm at 20 and 35°C herein lower than the solubility of amorphous silica divided by 10 at 20°C and by 16 at 35°C (Gunnarsson and Arnorsson, 2000). They remain lower than 1 ppm at 50°C and lower than 10 ppm at 70°C.

Initial dissolution rates as a function of pH and temperature are summarized in Table 4 (see Supplementary Material S1 and S2 for concentrations and S/V). According to Eq. (1), plotting log (r_0) as a function of pH allows to graphically determine the pH-dependency coefficient *n* of dissolution and the constant of the initial rate k_0 (Fig. 3a, Table 5). The dissolution rate does not follow the classical pH-dependency with the "U" trend usually observed during the dissolution of glasses (Gislason and Oelkers, 2003; Guy and Schott, 1989; Hamilton et al., 2001, 2001; Hellmann, 1994; Inagaki et al., 2013). Here, log r_0 linearly decreases with the increasing pH (Fig. 3a). Moreover, *n* coefficients are very low and glass dissolution does not seem to be highly pH-dependent (Table 5). Furthermore, in this study, it seems that *n* does not increase with temperature between 20 and 70°C (Table 5). Verney-Carron, 2008 found *n* coefficient independent of T for a Roman glass dissolution (between 15 and 90°C). Chen and Brantley, 1997 added data on the albite dissolution at several temperatures to complete other studies from Hellmann, 1994 and Chou and Wollast, 1984. Here again, results present *n* coefficients that seem to be T-independent between 5 and 300°C. However, Brady and

Walther, 1992 and Casey and Sposito, 1992 predicted that the pH-sensibility of dissolution can increase with an increasing temperature which was demonstrated by Chen and Brantley, 1998 for diopside ($CaMgSi_2O_6$) and anthophyllite ($(Mg,Fe)_7Si_8O_{22}(OH)_2$) dissolution between 25 and 90°C.

As the initial rate constant k_0 increases when T increases according to Arrhenius' law (Eq. 2) (Fig. 3b, Table 5), the activation energies *Ea*, as well as the associated uncertainties, were parameterized determined (Table 6). These data are similar to Sterpenich, 1998 who measures *Ea* value of 54 kJ.mol^{-1} at pH 5 for instance. According to Lasaga, 1981, determination of the activation energy *Ea* can be a method that indicates the mechanism controlling the glass alteration. Indeed, *Ea* is expected to range between 35 and 80 kJ.mol^{-1} for the dissolution of a silicate mineral when the reaction rate is controlled by surface reactions (e.g. Guy and Schott, 1989; Rimstidt and Barnes, 1980; Fleer, 1982; Criscenti et al., 2006). The activation energy *Ea* can vary with pH, as a function of surface charge (Guy and Schott, 1989; Casey and Sposito, 1992). Here, activation energy values are very similar for pH 3, 6, 8 and 10 (Table 6).

In order to parameterize the initial dissolution rate law as a function of T and pH, a fit of *n*, k_0 and *Ea* was carried out with Matlab software by using 16 data of r_0 (Table 4):

$$r_0 = 5.0 \times 10^6 [H^+]^{0.056} \exp\left(\frac{-39700}{RT}\right) \qquad \text{Eq. 9}$$

This fit has a coefficient of determination R^2 equal to 0.931. Constant k_0 is 5.0 ± 0.55 x 10^6 g.m^{-2}.d^{-1}, the pH-dependency coefficient *n* is 0.056 ± 0.009 and the activation energy *Ea* is 39.70 ± 0.03 kJ.mol^{-1}. Uncertainties were calculated by the software from the number of samples for a 95% confidence level. Figure 4a shows the 3D graphical representation of the initial rate law of dissolution as a function of T and pH. The variance (Fig. 4b) was analyzed. Two points present high deviations (almost 50%) due to an overestimation of r_0 by the rate law. Nevertheless, deviation average is 20% (Table 4).

3.3) Chemical affinity

In static condition, a drop in the dissolution rate is commonly observed and partly controlled by the gradual increase of Si concentration in solution, which leads to a decrease of the chemical affinity (Grambow, 1985). Since the altered layer is essentially composed of silica, we may assume that the drop in the dissolution rate is controlled by a silica phase. Amorphous silica, cristobalite-β or chalcedony are commonly used for dissolution rate laws of

314 silicate glasses (e.g. Frugier et al., 2008, 2018; Verney-Carron et al., 2010). In order to
315 determine this phase for SG3 glass, experimental NL_{Si} as a function of time were fitted using
316 the dissolution rate law and different solubility constants of silica phases (Eq. 4). These have
317 been calculated using the CHESS database and the Van't Hoff's law. The initial rate r_0 used is
318 the experimental one (r_0_exp in Table 4). The best fit is obtained with a chemical affinity term
319 associated with amorphous silica (SiO_2 (am)) (Fig. 5a). This is consistent with the data
320 obtained in Sessegolo et al. (2019) (Fig. 5b). Thus, a general dissolution rate law taking into
321 account pH, T and the chemical affinity can be determined:

322 $$r = 5.0 \times 10^{6}[H^{+}]^{0.056} \exp\left(\frac{-39700}{RT}\right)\left(1 - \frac{Q}{K_{SiO2(am)}}\right) \quad \text{Eq. 10}$$

323

324 *3.4) pH and T dependency of interdiffusion*

325 The determination of the potassium diffusion coefficient D_K for each data set of T and pH was
326 carried out by using the K concentration in solution and the second Fick's law (Eq. 8). Results
327 have allowed the interdiffusion rate law to be parameterized using Matlab software:

328 $$D_K = 2.4 \times 10^{-10}[H^{+}]^{0.25} \exp\left(\frac{-34500}{RT}\right) \quad \text{Eq. 11}$$

329 For these data (Table 7), the determination coefficient R^2 is 0.964. Diffusion constant D_0 is 2.4
330 ± 0.3 x 10^{-10} $m^2.s^{-1}$, pH-dependency n' is 0.25 ± 0.02 and Ea' is 34.5 ± 0.3 $kJ.mol^{-1}$.

331

332 *3.5) Characterization of the alteration layer*

333 The alteration patterns of the samples altered at 20 and 70°C were characterized to compare
334 the influence of extreme temperatures. Samples are named following "TpH" form for more
335 convenience; for example, a sample altered at pH 3 and T = 20°C will be called "20pH3".

336 Samples show higher degradations at 70°C than at 20°C (Fig. 6). At 20°C, the glass altered at
337 pH 3 has a scaly surface whereas the other samples present few visible changes to the naked
338 eye (Fig. 6). At 70°C, altered layer appears very thick and presents significant losses of
339 material revealing internal surfaces. 70pH8.5 appears less altered (Fig. 6).

340 Observation of glass surfaces using SEM confirms the presence of scales covering the entire
341 surface of 20pH3 (Fig. 7a). The altered layer is striated with channels, separated by dense and
342 developed cracks that are very interconnected. Different planes are visible, suggesting the
343 possibility of an alteration layer consisting of sub-layers parallel to each other, possibly with
344 loss of material and the departure of some outermost layers. Upper scales thus correspond
345 either to an outer layer that is almost entirely lost, or to scales that are detached and moved
346 during cutting of the sample. 20pH6.7 presents a heterogeneous surface with altered areas
347 (Fig. 7b) while others seem to be pristine. Finally, 20pH10 shows pits with unaltered edges

(Fig. 7c). At 70°C and acidic to near-neutral pH (70pH3, 70pH6.5), samples present an important scaling of the surface and the presence of secondary phases (Fig. 7d, e). The surface of 70pH8.5 only displays large and shallow craters.

The study of cross-sections is in agreement with alteration rates measured in the previous section. First, the alteration layer is thicker for samples at 70°C than at 20°C (Table 8, Fig. 8) due to the increase of alteration rates with temperature. Then, the more acidic the pH, the greater the alteration thickness *e* (Table 8). The alteration thickness of 70pH6 is higher than at pH 3 due to cracking of the reactors at the end of the experiment. Carbonation of the altering solution led to an acid pH of the solution while the 70pH3 solution was unbuffered, leading to a gradual increase of pH and a decrease of interdiffusion process. This implies thus a thinner altered layer. For 20pH10 and 70pH8.5, no altered layer is observable using SEM (Fig. 8). For 5 and 35°C at pH 10, the same observation is made (not shown here). These results are in agreement with the congruent dissolution that prevails in basic environments. When the solution is not saturated with silicon, the dissolution rate remains quite high and no hydrated layer or gel is formed.

EDS analyses confirmed the presence of a gel formed at acid and near-neutral pH with, in all cases, a high potassium leaching (K_2O ~2 wt.% in the alteration layer, Table 9). On the contrary, CaO can remain in relatively high concentration in the gel with sometimes more than 10 wt. %. Its retention is caused by over-saturation with hydroxylapatite and calcite in solution for some samples (Table 10). Al and Fe are insoluble few soluble and are therefore retained, increasing their relative concentration inside the alteration layer (Table 9). This is in accordance with very low NL_{Al} and NL_{Fe} observed in Fig. 1.

In an acidic medium, the release of alkaline and alkaline earth cations by interdiffusion is significant and causes over-saturation in solution with respect to some phases, particularly hydroxyapatite ($Ca_5(PO_4)_3(OH)$) as confirmed by JCHESS simulations (Table 10). SEM-EDS analyses show that the secondary phases observed at 70pH3 and 70pH6 are composed mainly of calcium and phosphorus (Fig. 9), which is in agreement with hydroxyapatite. XRD analyses confirm its presence and reveal the presence of other phases that are not easy to identify because of the width of some peaks (Fig. 10). Some of them can be attributed to the quartz and to the cristobalite α, which is in agreement with their saturation states (Table 10). However, the presence of quartz is unlikely due to its low precipitation rate. It is possible that this peak corresponds to an unidentified clay. Indeed, SEM-EDS analysis suggests the presence of zones inside the alteration layer composed of Si, Al and Mg (Fig. 9). The only mineral displaying a peak at 16.5° is the ammonioleucite ($(NH_4)(AlSi_2O_6)$). This phase can be consistent with the fact that solutions at pH 3 were acidified using HNO_3. It is known to replace analcime crystals $NaAlSi_2O_6{\cdot}H_2O$ (Yamada et al., 1998; Yuan et al., 2016). Finally, the presence of $CaCO_3$ was observed using SEM-EDS on some samples in small quantities. Thus, it is not excluded that the shoulder on the peak at 31° on XRD graph corresponds to the main peak of the vaterite but it is not very pronounced (Fig. 10).

The thickness of alteration layers observed using SEM was compared to the thickness calculated from the species concentrations in solution (Table 8). The normalized mass losses were divided by the density of the glass to obtain the theoretical thickness of the alteration layer (Table 8). NL_{Si} allows to estimate the glass thickness lost by dissolution. $NL_K - NL_{Si}$ and $NL_{Ca} - NL_{Si}$ correspond to the glass thickness that has only undergone hydration and interdiffusion, and therefore to the alteration layer thickness observed using SEM. The comparison between observations and calculations are quite consistent, particularly for $NL_{Ca} - NL_{Si}$. Nevertheless, for several samples, the gel thickness was difficult to be measured using SEM because of the high quantity of secondary phases.

4) Discussion

These experiments have allowed the rate laws for dissolution and interdiffusion to be determined. Parameters n, k_0, D_0, and Ea for the two laws can be compared with the values from literature on the same type of glass on the one hand, and on other glass compositions on the other hand.

To our knowledge, only Sterpenich (1998) carried out experiments in a water-saturated medium on medieval-type glasses (composition similar to SG3 glass: 52 wt.% SiO_2, 15 wt.% CaO, 15 wt.% K_2O) offering a comparison with our data (see below).

Table 11 presents different studies concerning other glass types (Advocat et al., 1990b; Chave et al., 2007; Guy and Schott, 1989; Inagaki et al., 2013; Verney-Carron et al., 2010). All values of n, Ea, k_0 and D_0 parameters are directly derived from publications, except in the case of Inagaki et al., 2013. For this latter, 16 dissolution rate values r_0 were provided in the article and then parameters were fitted with Matlab software, giving a coefficient of determination $R^2 = 0.991$. In order to better discern rate differences between glass compositions, it is possible to use n, Ea and k_0 of each author to trace the theoretical evolution of the dissolution rate as a function of the pH (Fig. 11a) in the defined range by the authors.

The dissolution rate r_0 of many glasses along with minerals' commonly follows a trend in "U" shape as a function of pH (Advocat et al., 1990a; Blum and Lasaga, 1991; Carroll-Webb and Walther, 1988; Gislason and Oelkers, 2003; Guy and Schott, 1989; Hamilton et al., 2001, 2001; Hellmann, 1994; Inagaki et al., 2013; Knauss and Wolery, 1986). The dissolution rate is high in acidic and basic medium and minimum at low-acidic/neutral pH (Advocat et al., 1990a; Blum and Lasaga, 1991; Gislason and Oelkers, 2003; Guy and Schott, 1989; Inagaki et al., 2013). The surface protonation model is commonly used with hydroxyl groups which are protonated or deprotonated as a function of pH. The minimum dissolution rate seems to be located at the point of zero net proton charge (pznpc), corresponding to the pH at which concentrations of positively and negatively charged sites are equal on the mineral surface (Brady and Walther, 1990; Carroll-Webb and Walther, 1988; Guy and Schott, 1989). For pH > pznpc, n coefficients measured in the literature are commonly negative, between -0.33 and -

0.40 (Table 11), whereas in our study, a weak and linear decrease of the log dissolution rate is observed on the pH range of 3 to 11, giving a positive *n* and a very low pH-dependency (*n* = 0.056) (Fig. 11a).

This specific behavior can be linked to the composition of the glass. It is very similar to the pH-dependency of Ca-Mg-silicates that highly differs from the behavior of aluminosilicates (Fig. 12). A linear decrease of the log dissolution rate with pH is observed for the dissolution rate of forsterite (Mg_2SiO_4) (Blum and Lasaga, 1988; Pokrovsky and Schott, 2000; Wogelius and Walther, 1991), enstatite ($Mg_2Si_2O_6$) (Oelkers and Schott, 2001; Schott et al., 1981), diopside ($CaMgSi_2O_6$) (Chen and Brantley, 1998; Schott et al., 1981), anthophyllite ($(Mg,Fe)_7Si_8O_{22}(OH)_2$) (Chen and Brantley, 1998) and wollastonite ($CaSiO_3$) (Weissbart and Rimstidt, 2000; Xie and Walther, 1994). Some minerals, like talc ($Mg_3Si_4O_{10}(OH)_2$), exhibit a log dissolution rate linearly decreasing in acid medium and then a dissolution rate pH-independent (Saldi et al., 2007).

According to Oelkers, 2001, the dissolution of glasses or minerals requires the breaking of several cation-oxygen bond types that occurs at different rates according to the cation. In this succession of steps, the slowest one is the rate limiting step. Especially the rate is higher in this order for alkalis > alkaline-earth elements > Al > Si at acid pH. However, each oxide has its own pH-dependency and this order can change at basic pH. Oelkers, 2001 has shown that the pH variation of the general dissolution rate could be deduced from the aqueous speciation of the last cation required to be removed to create the precursor complex. For several glasses (nuclear, basaltic) as well as minerals such as feldspars, pyroxenes or amphiboles, the alteration begins with the exchange of alkalis and alkaline-earth elements with hydrogenated species, which leads to the formation of a leached layer enriched in glass formers elements. Then, a two-stage dissolution process occurs: the partial removal of aluminum atoms with Al-O breaking by hydrogen and the release of partially detached Si tetrahedral. This is the reason why the far from equilibrium dissolution rates of the alkali feldspars or basaltic glasses for instance are observed to be linked to the Al solubility and proportional to the ratio $(a(H^+)/a(Al^{3+})^{1/3})$ (Gautier et al., 1994; Gislason and Oelkers, 2003). For basic silicates and certainly SG3 (with a very low Al content), the dissolution seems to be linked to the Ca solubility which decreases with pH.

Another way to explain the SG3 dissolution behavior can be the structure of the glass. Indeed, this particular behavior has also been observed by Mascaraque et al. 2017 on an aluminoborosilicate glass ($15Na_2O{\cdot}17Al_2O_3{\cdot}5B_2O_3{\cdot}63SiO_2$), an aluminosilicate glass ($15Na_2O.10CaO.15Al_2O_3.60SiO_2$) and a borosilicate glass ($15Na_2O{\cdot}10CaO{\cdot}15B_2O_3{\cdot}60SiO_2$). The authors have explained these results by linking the pH-dependency to the number of topological constraints of chemical topology. Phillips, 1979 and Phillips and Thorpe, 1985 have highlighted the existence of a balance between the number of freedom degrees of an atom and the number of interatomic stresses. Atomic network is said to be "flexible" if the number of topological constraints n_c is less than 3, "under constraints" or "rigid" if n_c is greater than 3,

and “isostatic” if the number of constraints is equal to 3. Mascaraque et al. 2017 have suggested that glasses with a high number of constraints per atom (n_c) have a low pH-dependency of dissolution because they are the most resistant to dissolution as each constraint acts as a spring. Glasses with low n_c exhibit internal deformation modes that are characterized by low energy barriers allowing water molecules to easily attack the network.

Intuitively, medieval glasses that are highly depolymerized and low durable (De Ferri et al., 2014; Melcher and Schreiner, 2006, 2005; Woisetschläger et al., 2000) should have a low n_c. It is possible to calculate this parameter for SG3 model glass. The method used is based on the counting of bond-stretching (BS) and bond-bending (BB) vibrations associated to each atom with its neighbors (Bauchy and Micoulaut, 2011; Gin et al., 2020). For network formers, numbers of BS and BB come from the coordination state of each atom and for modifier species, number of BS corresponds to their valency (Bauchy and Micoulaut, 2011. Gin et al., 2020). It is to be noted that the exact role and structure of iron and phosphorus in the structure of SG3 model glass is not known. Since it contains a high modifier content, it is assumed that Fe and P are both network-forming species. The yellow/orange color of SG3 seems to indicate that the iron is mostly on the Fe^{3+} state. It is assumed that Fe and P have a coordination number of 4 (Bingham et al., 2014; Cody et al., 2001). From these data, average number of bond-stretching per atom for SG3 glass is 1.2 and average number of bond-bending is 1.3, resulting in a number of constraints n_c of 2.5. This result is therefore in agreement with the low durability of medieval glass. However, according to the results of Mascaraque et al. 2017, the dissolution of SG3 glass should have a U-shape pH-dependency. Thus the results are not consistent with our study but this link between pH-dependency and n_c is not observed by Oey et al., 2017 on fly-ashes between pH 10 and 14 on a large range of nc (between 2.8 and 3.15). If it is easy to understand how the number of constraints can influence the magnitude of the dissolution rate, it can be less relevant to explain the pH-dependency that is linked to the solubility of each element.

4.3) Using kinetics parameters to model the alteration of stained glass windows

Numerical models are commonly used to simulate the evolution of systems by coupling transport of species and chemical reactions. They are widely used in geochemical fields with countless applications. Regarding the glass field, some authors developed and used models as GRAAL (Glass Reactivity with Allowance for the Alteration Layer, Frugier et al., 2009, 2008) or GM2001 (Grambow and Müller, 2001) to assess to the behavior and the long-term stability of nuclear glasses. It is necessary to develop models which *1)* reproduce the short-term behavior of glasses (validation of the model) and *2)* predict the long-term evolution of the system.

Medieval stained glass windows are another type of glass subjected to long-term alteration. To successfully model their alteration which occurs during hundreds of years can allow to access to the physicochemical transformations history. The consistency between the actual

state of stained glass windows and simulated ones will confirm our good understanding of the mechanisms involved in the deterioration of these glasses. In addition, it would then become possible to predict its future evolution, for instance in a case of global warming.

To model the glass alteration, it is necessary to know the chemical reactions occurring as well as the kinetics of these reactions. In the case of stained glass windows, if mechanisms were well known, parametric experiments and determination of kinetics as a function of pH, temperature and the saturation state of the solution have not yet been studied. Thus, with this present study, we have all the necessary information to develop a model relating to stained glass windows in contact with liquid water, therefore in contact with the rain for instance.

As a first step, simple calculations can be made. Considering that it rains 6 % of the time (MeteoFrance data), and considering a pH-range between 6 (usual pH of the rain) and 9 (increase due to interdiffusion), and an annual average temperature of 12°C, it is possible to use the dissolution rate law (Eq. 9) to estimate the loss of material between 500 and 700 µm, which is a significant part of the glass. However, the development of an alteration layer rapidly imposes a diffusion transport (Sessegolo et al., 2018; Verney-Carron et al., 2015). Now, by using the interdiffusion rate law (Eq. 11) with the same pH ad T parameters, D is $3.8 \cdot 10^{-18}$ $m^2.s^{-1}$ (at pH 6) and $6.8 \cdot 10^{-19}$ $m^2.s^{-1}$ (at pH 9). If it rains 6% of the time, after 650 years, this leads to 13 to 32 µm of alteration thickness. If we consider a higher percentage of time where the alteration layer remains humid, for example 25 %, the thickness is between 33 and 79 µm. These values are consistent with the low range of actual alteration layer thickness observations (between 40 and 250 µm, Lombardo et al., 2010; Sterpenich & Libourel, 2001; Carmona et al., 2006). These results highlight that in the future it will be necessary to use numerical models to simulate the evolution of systems by coupling chemical reactions and transport of species (e.g. Frugier et al., 2009; Verney-Carron et al., 2010). This would allow to precisely determine the pH of the solution in contact with the glass as a function of the rain flow, composition, pH, or the pH evolution inside the alteration layer. Then, simple calculations show that the inclusion of the alteration caused by water vapor with the relative humidity as a key factor is necessary to be completely explain the alteration. Indeed, this kind of alteration is not negligible (Sessegolo et al., 2018). The use of chemistry-transport models with parametric laws would be useful.

Conclusion

Previous studies of the literature have investigated the alteration of stained glass windows to identify alteration products and determine alteration mechanisms. This study was focused on alteration kinetics associated to these mechanisms and has determined the rate laws as a function of different parameters such as pH, temperature and saturation state of the altering

solution. These laws can now be implemented in a model to perform geochemical simulations of the alteration of stained-glass windows subject to rainfall.

The determined parameters can be compared to the panel of rate laws established for other glass compositions (nuclear, roman and basaltic). The activation energies of alteration processes are very similar to other glasses. The surprising result is that Si-K-Ca medieval glasses have a very low pH dependency at alkaline pH, similarly to previous results and to the behavior of basic silicates. This requires further structural studies to understand the origin of this particular behavior.

Acknowledgements

The authors would like to thank the French National Research Agency (ANR) for their financial support (ANR GLAM).

Competing interests

The authors declare no competing interests.

References

Aagaard, P., Helgeson, H.C., 1982. Thermodynamic and kinetic constraints on reaction rates among minerals and aqueous solutions; I, Theoretical considerations. Am. J. Sci. 282, 237–285. https://doi.org/10.2475/ajs.282.3.237

Advocat, T., Crovisier, J.L., Fritz, B., Vernaz, E., 1989. Thermokinetic Model of Borosilicate Glass Dissolution: Contextual Affinity. MRS Online Proc. Libr. Arch. 176. https://doi.org/10.1557/PROC-176-241

Advocat, T., Crovisier, J.L., Vernaz, E., Ehret, G., Charpentier, H., 1990. Hydrolysis of R7T7 Nuclear Waste Glass in Dilute Media: Mechanisms and Rate as a function of Ph. MRS Online Proc. Libr. Arch. 212. https://doi.org/10.1557/PROC-212-57

Bauchy, M., Micoulaut, M., 2011. Atomic scale foundation of temperature-dependent bonding constraints in network glasses and liquids. J. Non-Cryst. Solids, STRUCTURE OF NON-CRYSTALLINE MATERIALS 11 Proceedings of the 11th Conference on the Structure of Non-Crystalline Materials (NCM11) Paris, France June 28- July 2, 2010 357, 2530–2537. https://doi.org/10.1016/j.jnoncrysol.2011.03.017

Bingham, P.A., Hannant, O.M., Reeves-McLaren, N., Stennett, M.C., Hand, R.J., 2014. Selective behaviour of dilute Fe3+ ions in silicate glasses: an Fe K-edge EXAFS and XANES study. J. Non-Cryst. Solids 387, 47–56. https://doi.org/10.1016/j.jnoncrysol.2013.12.034

Blum, A., Lasaga, A., 1988. Role of surface speciation in the low-temperature dissolution of minerals. Nature 331, 431. https://doi.org/10.1038/331431a0

576 Blum, A.E., Lasaga, A.C., 1991. The role of surface speciation in the dissolution of albite.
577 Geochim. Cosmochim. Acta 55, 2193–2201. https://doi.org/10.1016/0016-
578 7037(91)90096-N
579 Brady, P.V., Walther, J.V., 1992. Surface chemistry and silicate dissolution at elevated
580 temperatures. Am. J. Sci. 292, 639–658. https://doi.org/10.2475/ajs.292.9.639
581 Brady, P.V., Walther, J.V., 1990. Kinetics of quartz dissolution at low temperatures. Chem.
582 Geol. 82, 253–264. https://doi.org/10.1016/0009-2541(90)90084-K
583 Cody, G.D., Mysen, B., Sághi-Szabó, G., Tossell, J.A., 2001. Silicate-phosphate interactions in silicate glasses
584 and melts: I. A multinuclear (27Al,29Si,31P) MAS NMR and ab initio chemical shielding (31P) study
585 of phosphorous speciation in silicate glasses. Geochim. Cosmochim. Acta 65, 2395–2411.
586 https://doi.org/10.1016/S0016-7037(01)00597-X
587 Carmona, N., Villegas, M.A., Navarro, J.M.F., 2006. Characterisation of an intermediate decay
588 phenomenon of historical glasses. J. Mater. Sci. 41, 2339–2346.
589 https://doi.org/10.1007/s10853-005-3948-6
590 Carroll-Webb, S.A., Walther, J.V., 1988. A surface complex reaction model for the pH-
591 dependence of corundum and kaolinite dissolution rates. Geochim. Cosmochim. Acta
592 52, 2609–2623. https://doi.org/10.1016/0016-7037(88)90030-0
593 Casey, W.H., Lasaga, A.C., Gibbs, G.V., 1990. Mechanisms of silica dissolution as inferred from
594 the kinetic isotope effect. Geochim. Cosmochim. Acta 54, 3369–3378.
595 https://doi.org/10.1016/0016-7037(90)90291-R
596 Casey, W.H., Sposito, G., 1992. On the temperature dependence of mineral dissolution rates.
597 Geochim. Cosmochim. Acta 56, 3825–3830. https://doi.org/10.1016/0016-
598 7037(92)90173-G
599 Chave, T., Frugier, P., Ayral, A., Gin, S., 2007. Solid state diffusion during nuclear glass residual
600 alteration in solution. J. Nucl. Mater. 362, 466–473.
601 https://doi.org/10.1016/j.jnucmat.2007.01.095
602 Chen, Y., Brantley, S.L., 1998. Diopside and anthophyllite dissolution at 25° and 90°C and acid
603 pH. Chem. Geol. 147, 233–248. https://doi.org/10.1016/S0009-2541(98)00016-3
604 Chen, Y., Brantley, S.L., 1997. Temperature- and pH-dependence of albite dissolution rate at
605 acid pH. Chem. Geol. 135, 275–290. https://doi.org/10.1016/S0009-2541(96)00126-X
606 Chou, L., Wollast, R., 1984. Study of the weathering of albite at room temperature and
607 pressure with a fluidized bed reactor. Geochim. Cosmochim. Acta 48, 2205–2217.
608 https://doi.org/10.1016/0016-7037(84)90217-5
609 Criscenti, L.J., Kubicki, J.D., Brantley, S.L., 2006. Silicate glass and mineral dissolution:
610 calculated reaction paths and activation energies for hydrolysis of a q3 si by H3O+
611 using ab initio methods. J. Phys. Chem. A 110, 198–206.
612 https://doi.org/10.1021/jp044360a
613 Crovisier, J.L., Fritz, B., Grambow, B., Eberhart, J.P., 1985. Dissolution of Basaltic Glass in
614 Seawater : Experiments and Thermodynamic Modelling. MRS Online Proc. Libr. Arch.
615 50. https://doi.org/10.1557/PROC-50-273
616 Crovisier, J.L., Honnorez, J., Eberhart, J.P., 1987. Dissolution of basaltic glass in seawater:
617 Mechanism and rate. Geochim. Cosmochim. Acta 51, 2977–2990.
618 https://doi.org/10.1016/0016-7037(87)90371-1
619 De Ferri, L., Lottici, P.P., Vezzalini, G., 2014. Characterization of alteration phases on Potash–
620 Lime–Silica glass. Corros. Sci. 80, 434–441.
621 https://doi.org/10.1016/j.corsci.2013.11.068
622 Debure, M., De Windt, L., Frugier, P., Gin, S., 2013. HLW glass dissolution in the presence of
623 magnesium carbonate: Diffusion cell experiment and coupled modeling of diffusion

and geochemical interactions. J. Nucl. Mater. 443, 507–521. https://doi.org/10.1016/j.jnucmat.2013.07.068

Doremus, R.H., 1975. Interdiffusion of hydrogen and alkali ions in a glass surface. J. Non-Cryst. Solids, Glass Surfaces 19, 137–144. https://doi.org/10.1016/0022-3093(75)90079-4

Dove, P.M., Crerar, D.A., 1990. Kinetics of quartz dissolution in electrolyte solutions using a hydrothermal mixed flow reactor. Geochim. Cosmochim. Acta 54, 955–969. https://doi.org/10.1016/0016-7037(90)90431-J

Fleer, V.N., 1982. The dissolution kinetics of anortite (CaAl2Si2O8) and synthetic strontium feldspar (SrAl2Si2O8) in aqueous solutions at tempartures below 100°C: With application to the geological disposal of radioactive nuclear wastes. Pa. State Univ., University Park.

Frugier, P., Chave, T., Gin, S., Lartigue, J.-E., 2009. Application of the GRAAL model to leaching experiments with SON68 nuclear glass in initially pure water. J. Nucl. Mater. 392, 552–567. https://doi.org/10.1016/j.jnucmat.2009.04.024

Frugier, P., Gin, S., Minet, Y., Chave, T., Bonin, B., Godon, N., Lartigue, J.-E., Jollivet, P., Ayral, A., De Windt, L., Santarini, G., 2008. SON68 nuclear glass dissolution kinetics: Current state of knowledge and basis of the new GRAAL model. J. Nucl. Mater. 380, 8–21. https://doi.org/10.1016/j.jnucmat.2008.06.044

Garcia Vallès, M., Vendrell Saz, M., 2002. The glasses of the transept's rosette of the Cathedral of Tarragona: characterization, classification and decay. Boletin Soc. Espanola Ceram. Vidr. 41, 217–224.

Gin, S., Wang, M., Bisbrouck, N., Taron, M., Lu, X., Deng, L., Angeli, F., Charpentier, T., Delaye, J.-M., Du, J., Bauchy, M., 2020. Can a simple topological-constraints-based model predict the initial dissolution rate of borosilicate and aluminosilicate glasses? Npj Mater. Degrad. 4, 1–10. https://doi.org/10.1038/s41529-020-0111-4

Gin, S., Collin, M., Jollivet, P., Fournier, M., Minet, Y., Dupuy, L., Mahadevan, T., Kerisit, S., Du, J., 2018. Dynamics of self-reorganization explains passivation of silicate glasses. Nat. Commun. 9, 2169. https://doi.org/10.1038/s41467-018-04511-2

Gin, S., Jollivet, P., Fournier, M., Berthon, C., Wang, Z., Mitroshkov, A., Zhu, Z., Ryan, J.V., 2015. The fate of silicon during glass corrosion under alkaline conditions: A mechanistic and kinetic study with the International Simple Glass. Geochim. Cosmochim. Acta 151, 68–85. https://doi.org/10.1016/j.gca.2014.12.009

Gislason, S.R., Oelkers, E.H., 2003. Mechanism, rates, and consequences of basaltic glass dissolution: II. An experimental study of the dissolution rates of basaltic glass as a function of pH and temperature. Geochim. Cosmochim. Acta 67, 3817–3832. https://doi.org/10.1016/S0016-7037(03)00176-5

Golubev, S.V., Pokrovsky, O.S., Schott, J., 2005. Experimental determination of the effect of dissolved CO2 on the dissolution kinetics of Mg and Ca silicates at 25 °C. Chem. Geol. 217, 227–238. https://doi.org/10.1016/j.chemgeo.2004.12.011

Grambow, B., 1984. A General Rate Equation for Nuclear Waste Glass Corrosion. MRS Online Proc. Libr. Arch. 44. https://doi.org/10.1557/PROC-44-15

Gunnarsson, I., Arnórsson, S., 2000. Amorphous silica solubility and the thermodynamic properties of H4SiO°4 in the range of 0° to 350°C at Psat. Geochim. Cosmochim. Acta 64, 2295–2307. https://doi.org/10.1016/S0016-7037(99)00426-3

Guy, C., Schott, J., 1989. Multisite surface reaction versus transport control during the hydrolysis of a complex oxide. Chem. Geol., Kinetic Geochemistry 78, 181–204. https://doi.org/10.1016/0009-2541(89)90057-0

Hamilton, J.P., Brantley, S.L., Pantano, C.G., Criscenti, L.J., Kubicki, J.D., 2001. Dissolution of nepheline, jadeite and albite glasses: toward better models for aluminosilicate

673 dissolution. Geochim. Cosmochim. Acta 65, 3683–3702.
674 https://doi.org/10.1016/S0016-7037(01)00724-4
675 Hellmann, R., 1997. The albite-water system: Part IV. Diffusion modeling of leached and
676 hydrogen-enriched layers. Geochim. Cosmochim. Acta 61, 1595–1611.
677 https://doi.org/10.1016/S0016-7037(97)00023-9
678 Hellmann, R., 1994. The albite-water system: Part I. The kinetics of dissolution as a function of
679 pH at 100, 200 and 300°C. Geochim. Cosmochim. Acta 58, 595–611.
680 https://doi.org/10.1016/0016-7037(94)90491-X
681 Houser, C. A., Herman, J.S., Tsong, I.S.T., White, W.B., Lanford, W.A., 1980. Sodium-hydrogen
682 interdiffusion in sodium silicate glasses. J. Non-Crystaline Silids 41, 89–98.
683 Inagaki, Y., Kikunaga, T., Idemitsu, K., Arima, T., 2013. Initial Dissolution Rate of the
684 International Simple Glass as a Function of pH and Temperature Measured Using
685 Microchannel Flow-Through Test Method. Int. J. Appl. Glass Sci. 4, 317–327.
686 https://doi.org/10.1111/ijag.12043
687 Knauss, K.G., Wolery, T.J., 1986. Dependence of albite dissolution kinetics on ph and time at
688 25°c and 70°c. Geochim. Cosmochim. Acta 50, 2481–2497.
689 https://doi.org/10.1016/0016-7037(86)90031-1
690 Lanford, W.A., Davis, K., Lamarche, P., Laursen, T., Groleau, R., Doremus, R.H., 1979.
691 Hydration of soda-lime glass. J. Non-Cryst. Solids 33, 249–266.
692 Lasaga, A., 1981. Rate laws of chemical reactions in Kinetics of Geochemical Processes,
693 Mineralogical Society of America. ed. A. C. Lasaga and R. J. Kirkpatrick, Washington D.
694 C.
695 Lombardo, T., Gentaz, L., Verney-Carron, A., Chabas, A., Loisel, C., Neff, D., Leroy, E., 2013.
696 Characterisation of complex alteration layers in medieval glasses. Corros. Sci. 72, 10–
697 19. https://doi.org/10.1016/j.corsci.2013.02.004
698 Lombardo, T., Loisel, C., Gentaz, L., Chabas, A., Verita, M., Pallot-Frossard, I., 2010. Long term
699 assessment of atmospheric decay of stained glass windows. Corros. Eng. Sci. Technol.
700 45, 420–424. https://doi.org/10.1179/147842210X12710800383800
701 Mascaraque, N., Bauchy, M., Smedskjaer, M.M., 2017. Correlating the Network Topology of
702 Oxide Glasses with their Chemical Durability. J. Phys. Chem. B 121, 1139–1147.
703 https://doi.org/10.1021/acs.jpcb.6b11371
704 Maurer, C., Clark, D.E., Hench, L.L., Grambow, B., 1985. Solubility effects on the corrosion of
705 nuclear defense waste glasses. Nucl. Chem. Waste Manag. 5, 193–201.
706 https://doi.org/10.1016/0191-815X(85)90078-6
707 Melcher, M., Schreiner, M., 2006. Leaching studies on naturally weathered potash-lime–silica
708 glasses. J. Non-Cryst. Solids 352, 368–379.
709 https://doi.org/10.1016/j.jnoncrysol.2006.01.017
710 Melcher, M., Schreiner, M., 2005. Evaluation procedure for leaching studies on naturally weathered potash-lime-
711 silica glasses with medieval composition by scanning electron microscopy. J. Non-Cryst. Solids 351,
712 1210–1225. https://doi.org/10.1016/j.jnoncrysol.2005.02.020
713 Menz, F.C., Seip, H.M., 2004. Acid rain in Europe and the United States: an update. Environ.
714 Sci. Policy 7, 253–265. https://doi.org/10.1016/j.envsci.2004.05.005
715 Oelkers, E.H., 2001. General kinetic description of multioxide silicate mineral and glass dissolution. Geochim.
716 Cosmochim. Acta 65, 3703–3719. https://doi.org/10.1016/S0016-7037(01)00710-4
717 Oelkers, E.H., Schott, J., 2001. An experimental study of enstatite dissolution rates as a
718 function of pH, temperature, and aqueous Mg and Si concentration, and the
719 mechanism of pyroxene/pyroxenoid dissolution. Geochim. Cosmochim. Acta 65,
720 1219–1231. https://doi.org/10.1016/S0016-7037(00)00564-0

Oey, T., Hsiao, Y.-H., Callagon, E., Wang, B., Pignatelli, I., Bauchy, M., Sant, G.N., 2017. Rate controls on silicate dissolution in cementitious environments. RILEM Tech. Lett. 2, 67–73. https://doi.org/10.21809/rilemtechlett.2017.35

Petit, J.-C., Mea, G.D., Dran, J.-C., Magonthier, M.-C., Mando, P.A., Paccagnella, A., 1990. Hydrated-layer formation during dissolution of complex silicate glasses and minerals. Geochim. Cosmochim. Acta 54, 1941–1955. https://doi.org/10.1016/0016-7037(90)90263-K

Phillips, J.C., 1979. Topology of covalent non-crystalline solids I: Short-range order in chalcogenide alloys. J. Non-Cryst. Solids 34, 153–181. https://doi.org/10.1016/0022-3093(79)90033-4

Phillips, J.C., Thorpe, M.F., 1985. Constraint theory, vector percolation and glass formation. Solid State Commun. 53, 699–702. https://doi.org/10.1016/0038-1098(85)90381-3

Pokrovsky, O.S., Schott, J., 2000. Kinetics and mechanism of forsterite dissolution at 25°C and pH from 1 to 12. Geochim. Cosmochim. Acta 64, 3313–3325. https://doi.org/10.1016/S0016-7037(00)00434-8

Rimstidt, J.D., Barnes, H.L., 1980. The kinetics of silica-water reactions. Geochim. Cosmochim. Acta 44, 1683–1699. https://doi.org/10.1016/0016-7037(80)90220-3

Saldi, G.D., Köhler, S.J., Marty, N., Oelkers, E.H., 2007. Dissolution rates of talc as a function of solution composition, pH and temperature. Geochim. Cosmochim. Acta 71, 3446–3457. https://doi.org/10.1016/j.gca.2007.04.015

Schalm, O., Anaf, W., 2016. Laminated altered layers in historical glass: Density variations of silica nanoparticle random packings as explanation for the observed lamellae. J. Non-Cryst. Solids 442, 1–16. https://doi.org/10.1016/j.jnoncrysol.2016.03.019

Schalm, O., Janssens, K., Wouters, H., Caluwé, D., 2007. Composition of 12–18th century window glass in Belgium: Non-figurative windows in secular buildings and stained-glass windows in religious buildings. Spectrochim. Acta Part B At. Spectrosc., A Collection of Papers Presented at the 18th International Congress on X-Ray Optics and Microanalysis (ICXOM 2005) 62, 663–668. https://doi.org/10.1016/j.sab.2007.03.006

Schott, J., Berner, R.A., Sjöberg, E.L., 1981. Mechanism of pyroxene and amphibole weathering—I. Experimental studies of iron-free minerals. Geochim. Cosmochim. Acta 45, 2123–2135. https://doi.org/10.1016/0016-7037(81)90065-X

Sessegolo, L., Verney-Carron, A., Ausset, P., Saheb, M., Chabas, A., 2019. Effect of surface roughness on medieval-type glass alteration in aqueous medium. J. Non-Cryst. Solids 505, 260–271. https://doi.org/10.1016/j.jnoncrysol.2018.10.051

Sessegolo, L., Verney-Carron, A., Saheb, M., Remusat, L., Gonzalez-Cano, A., Nuns, N., Mertz, J.-D., Loisel, C., Chabas, A., 2018. Long-term weathering rate of stained-glass windows using H and O isotopes. Npj Mater. Degrad. 2, 17. https://doi.org/10.1038/s41529-018-0038-1

Singh, S., Elumalai, S.P., Pal, A.K., 2016. Rain pH estimation based on the particulate matter pollutants and wet deposition study. Sci. Total Environ. 563–564, 293–301. https://doi.org/10.1016/j.scitotenv.2016.04.066

Sterpenich, J., 1998. Altération des vitraux médiévaux. Contribution à l'étude du comportement à long terme des verres de confinement.

Sterpenich, J., Libourel, G., 2006. Water diffusion in silicate glasses under natural weathering conditions: evidence from buried medieval stained glasses. J. Non-Cryst. Solids 352, 5446–5451. https://doi.org/10.1016/j.jnoncrysol.2006.08.041

Sterpenich, J., Libourel, G., 2001. Using stained glass windows to understand the durability of toxic waste matrices. Chem. Geol., 6th International Silicate Melt Workshop 174, 181–193. https://doi.org/10.1016/S0009-2541(00)00315-6

Tournié, A., Majérus, O., Lefèvre, G., Rager, M.N., Walmé, S., Caurant, D., Barboux, P., 2013. Impact of boron complexation by Tris buffer on the initial dissolution rate of borosilicate glasses. J. Colloid Interface Sci. 400, 161–167. https://doi.org/10.1016/j.jcis.2013.03.009

Valle, N., Verney-Carron, A., Sterpenich, J., Libourel, G., Deloule, E., Jollivet, P., 2010. Elemental and isotopic (29Si and 18O) tracing of glass alteration mechanisms. Geochim. Cosmochim. Acta 74, 3412–3431. https://doi.org/10.1016/j.gca.2010.03.028

van der Lee, J., De Windt, L., 2002. CHESS tutorial and Cookbook. Updated for version 3.0. Ecole des Mines de Paris, Centre d'Informatique Géologique, Fontainebleau, France.

van der Lee, J., De Windt, L., Lagneau, V., Goblet, P., 2003. Module-oriented Modeling of Reactive Transport with HYTEC. Comput Geosci 29, 265–275. https://doi.org/10.1016/S0098-3004(03)00004-9

van der Lee, J., De Windt, L., Lagneau, V., Goblet, P., 2002. Presentation and application of the reactive transport code HYTEC, in: Hassanizadeh, S.M., Schotting, R.J., Gray, W.G., Pinder, G.F. (Eds.), Developments in Water Science, Computational Methods in Water Resources. Elsevier, pp. 599–606. https://doi.org/10.1016/S0167-5648(02)80114-9

Verney-Carron, A., 2008. Étude d'analogues archéologiques pour la validation des modèles de comportement à long terme des verres nucléaires. Vandoeuvre-les-Nancy, INPL.

Verney-Carron, A., Gin, S., Frugier, P., Libourel, G., 2010. Long-term modeling of alteration-transport coupling: Application to a fractured Roman glass. Geochim. Cosmochim. Acta 74, 2291–2315. https://doi.org/10.1016/j.gca.2010.01.001

Verney-Carron, A., Saheb, M., Loisel, C., Duhamel, R., Remusat, L., 2015. Use of Hydrogen Isotopes to Understand Stained Glass Weathering. Procedia Earth Planet. Sci., 11th Applied Isotope Geochemistery Conference AIG-11 13, 64–67. https://doi.org/10.1016/j.proeps.2015.07.015

Verney-Carron, A., Sessegolo, L., Saheb, M., Valle, N., Ausset, P., Losno, R., Mangin, D., Lombardo, T., Chabas, A., Loisel, C., 2017. Understanding the mechanisms of Si–K–Ca glass alteration using silicon isotopes. Geochim. Cosmochim. Acta 203, 404–421. https://doi.org/10.1016/j.gca.2017.01.030

Wassick, T.A., Doremus, R.H., Lanford, W.A., Burman, C., 1983. Hydration of soda-lime silicate glass, effect of alumina. J. Non-Cryst. Solids 54, 139–151.

Weissbart, E.J., Rimstidt, J.D., 2000. Wollastonite: Incongruent dissolution and leached layer formation. Geochim. Cosmochim. Acta 64, 4007–4016. https://doi.org/10.1016/S0016-7037(00)00475-0

Wogelius, R.A., Walther, J.V., 1991. Olivine dissolution at 25°C: Effects of pH, CO2, and organic acids. Geochim. Cosmochim. Acta 55, 943–954. https://doi.org/10.1016/0016-7037(91)90153-V

Woisetschläger, G., Dutz, M., Paul, S., Schreiner, M., 2000. Weathering phenomena on naturally weathered potash-lime-silica-glass with medieval composition studied by secondary electron microscopy and energy dispersive microanalysis. Microchim. Acta 135, 121–130.

Xie, Z., Walther, J.V., 1994. Dissolution stoichiometry and adsorption of alkali and alkaline earth elements to the acid-reacted wollastonite surface at 25°C. Geochim. Cosmochim. Acta 58, 2587–2598. https://doi.org/10.1016/0016-7037(94)90130-9

Yamada, M., Miyawaki, R., Nakai, I., Izumi, F., Nagashima, K., 1998. A rietveld analysis of the crystal structure of ammonioleucite. Mineral. J. 20, 105–112. https://doi.org/10.2465/minerj.20.105

Yuan, J., Yang, J., Ma, H., Liu, C., 2016. Crystal structural transformation and kinetics of NH4+/Na+ ion-exchange in analcime. Microporous Mesoporous Mater. 222, 202–208. https://doi.org/10.1016/j.micromeso.2015.10.020

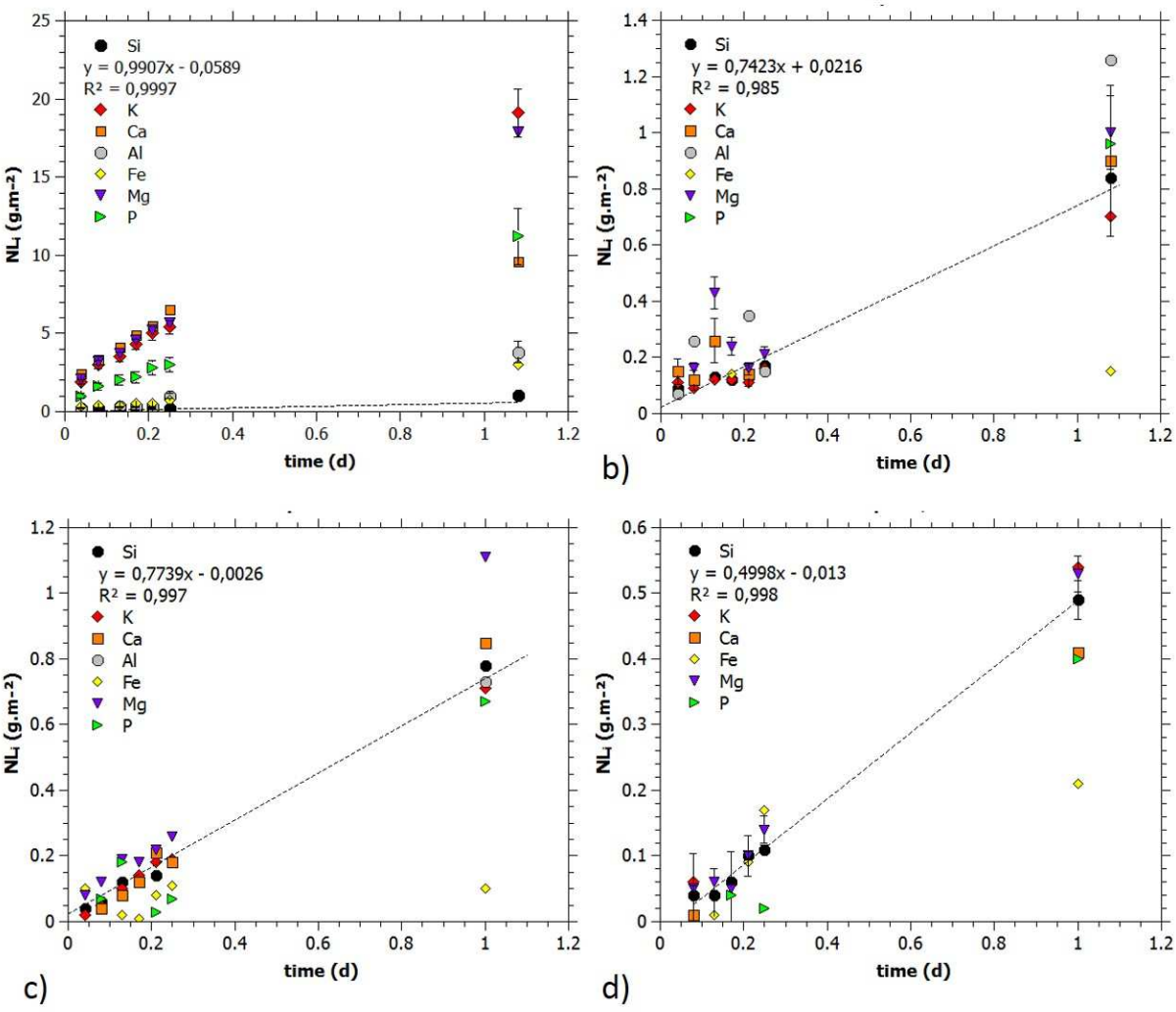

Figure 1. Normalized mass losses of glass elements *i* (NL_i in $g.m^{-2}$) for samples altered at 50°C at pH: a) 2.0 b) 5.4 c) 6.3 and d) 9.8 for 24 h in static condition. Black regression lines correspond to Si evolution. Uncertainties are low and corresponding error bars are sometimes smaller than symbols.

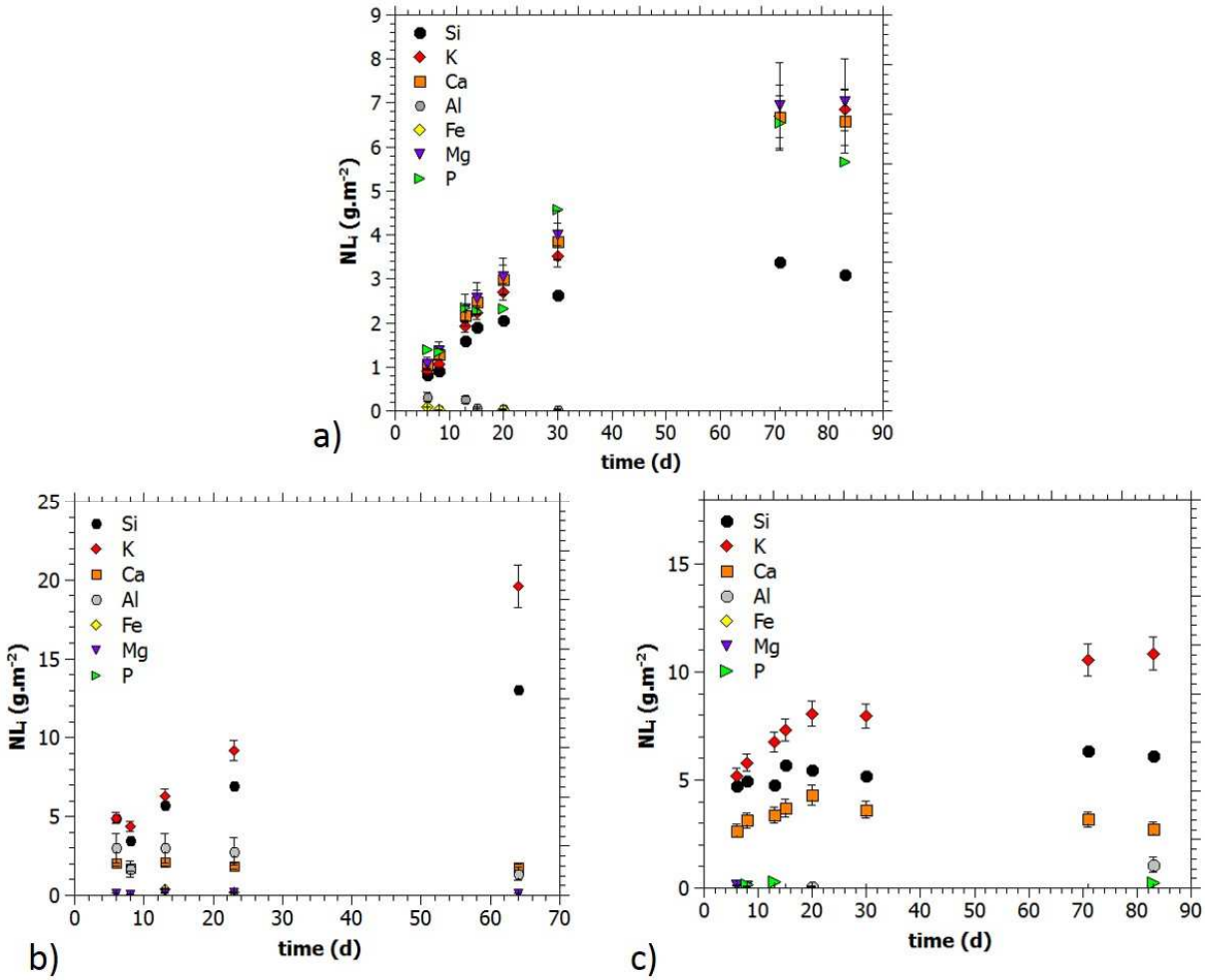

Figure 2. Normalized mass losses of glass elements *i* (NL_i in $g.m^{-2}$) for samples altered at a) 20°C and pH 10.3, b) 70°C at pH 9.8 and c) 70°C at pH 10.4 in static condition. Uncertainties can be low and corresponding error bars are sometimes smaller than symbols. For c) numerous elemental concentrations were lower than the quantification limits.

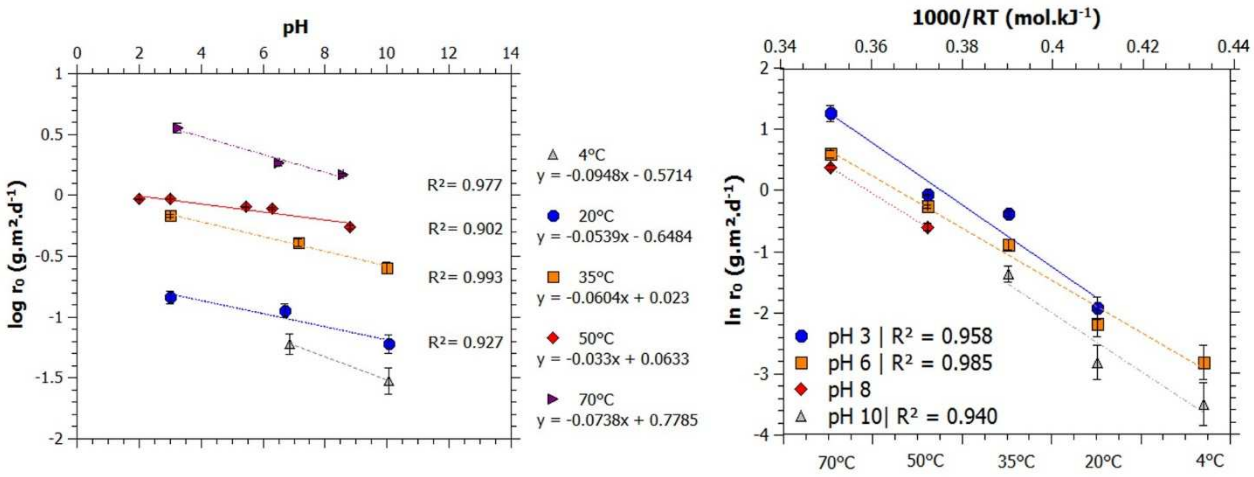

Figure 3. *a)* Logarithm of initial dissolution rate r_0 (in $g.m^{-2}.d^{-1}$) as a function of pH for the experiments at 20, 35, 50 and 70°C. *b)* Natural logarithm of initial dissolution rate r_0 (in $g.m^{-2}.d^{-1}$) as a function of 1000/RT (in $mol.kJ^{-1}$) for pH 3, 6, 8 and 10. Values of n, k_0 and Ea are indicated in Tables 5 and 5.

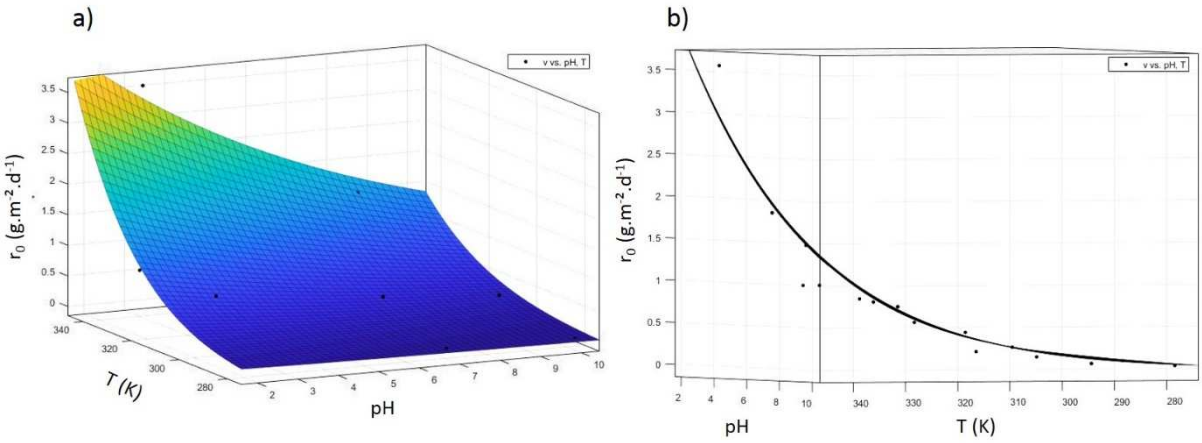

Figure 4. Fit of experimental data (using Matlab software). Black points correspond to r_0 measurements. a) 3D representation of the initial dissolution rate law (in g.m^{-2}.d^{-1}) as a function of pH and temperature (in K). b) Side view of the discrepancy between the experimental values and the rate law.

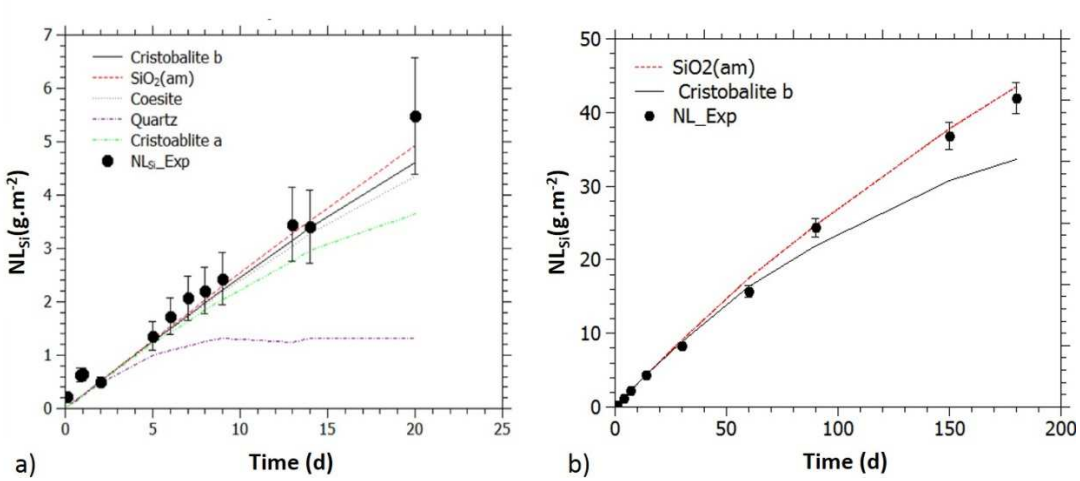

Figure 5. Fits of experimental NL_{Si} (black points) with dissolution rate law (Eq. 4) including r_0_measured (Table 4) and several silica phases tested for the chemical affinity term. a) Sample altered at pH 10 and 35°C during 20 days. b) Fit of experimental NL_{Si} from Sessegolo et al., 2019.

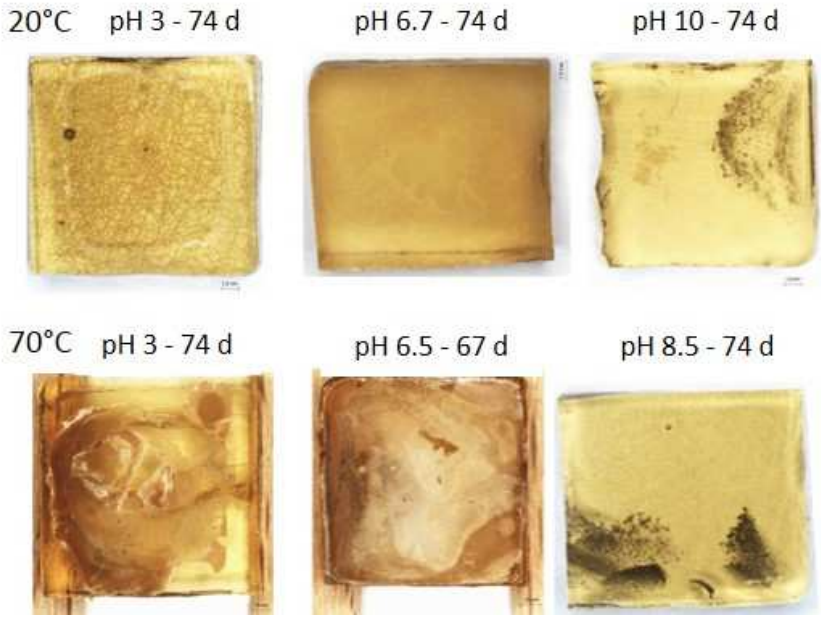

Figure 6. Photographs of surfaces of altered samples at 20 and 70°C at pH 3.0, 6.5, 8.5 and 10.0 after 74 days for all except 70pH6.5 (67 days). Samples are 1.25 x 1.25 x 0.3 cm^3. Darker areas on 20pH10 and 70pH8.5 are bubbles formed in the bulk of the glass during synthesis.

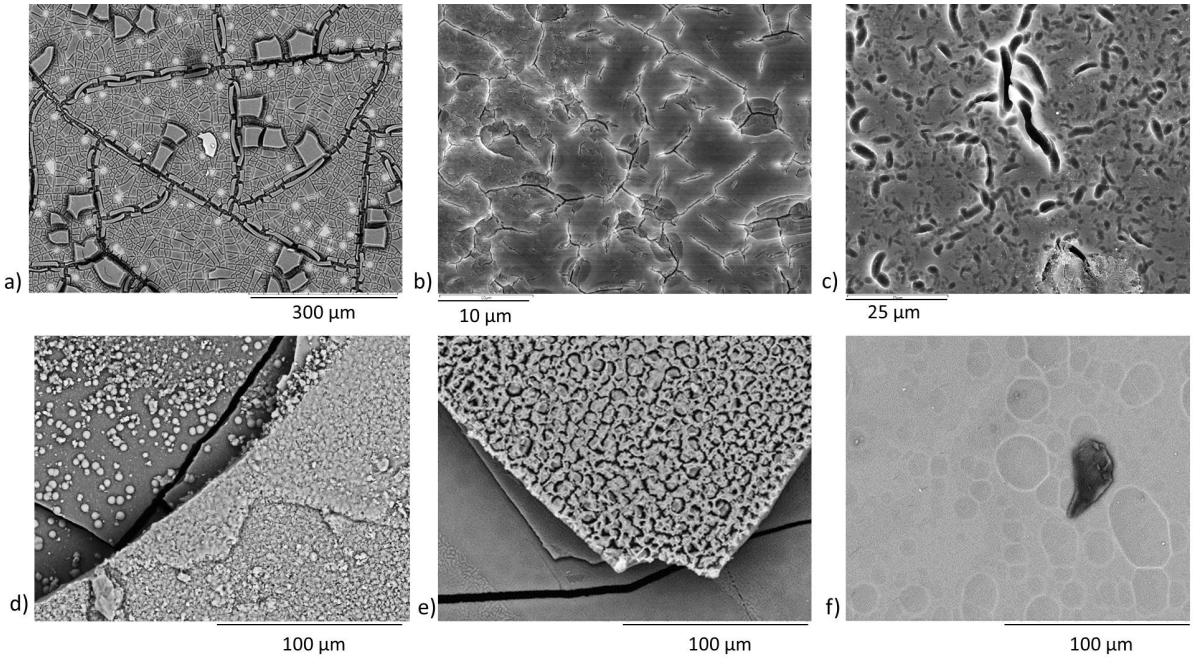

Figure 7. SEM-BSE images of the previous surfaces of a) 20pH3, b) 20pH6.7, c) 20pH10, d) 70pH3, e) 70pH6.5 and f) 70pH8.5.

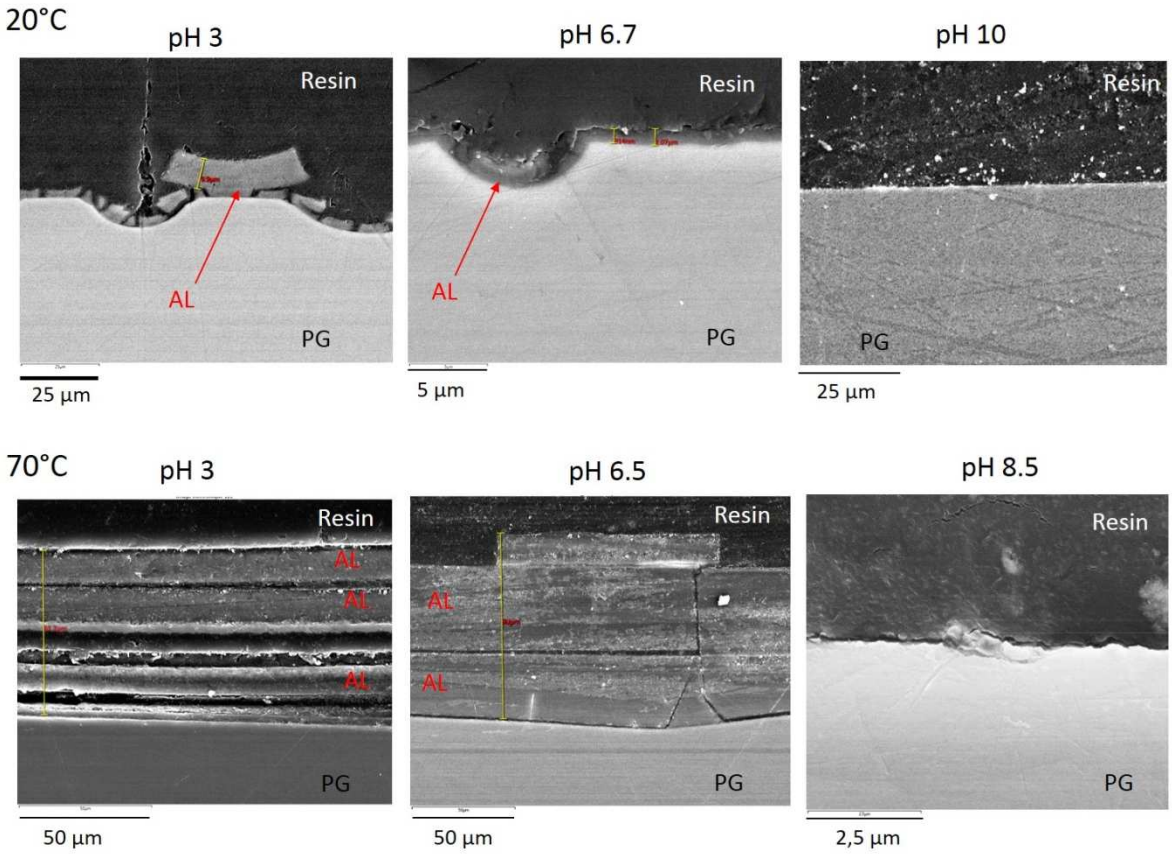

Figure 8. SEM-SE cross-sections images of samples altered at 20 and 70°C during 74 days (67 days for 70pH6.5). "AL" means Altered Layer and “PG” means Pristine Glass.

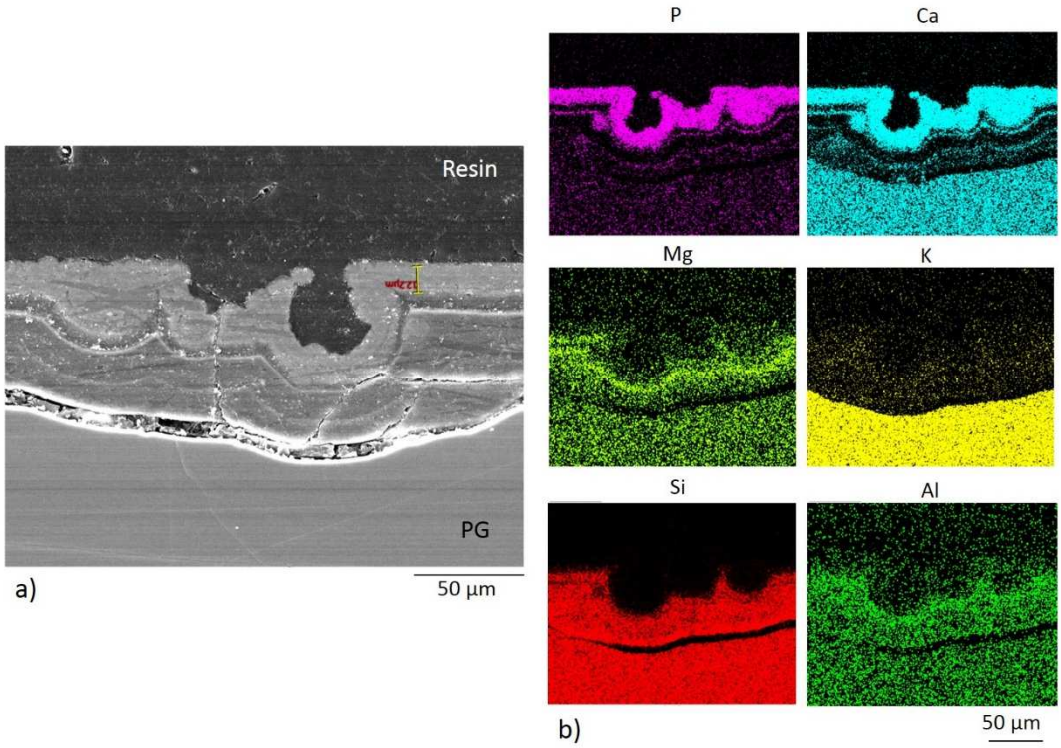

Figure 9. 70pH6.5 SEM-EDS analysis after 67 days of alteration. a) SEM-BSE image of the alteration layer, b) EDS mapping.

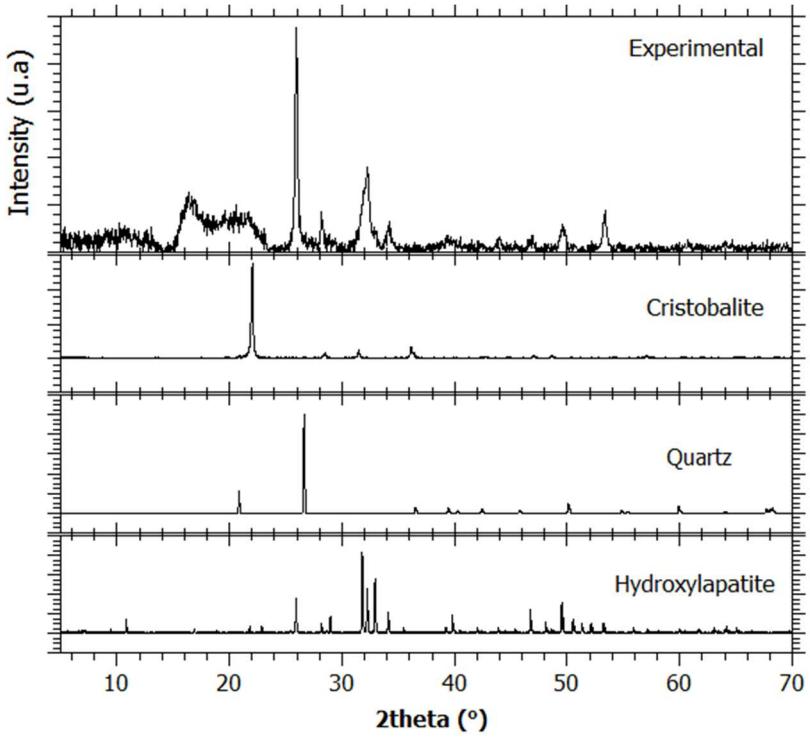

Figure 10. Diffractogram of experimental phases present on the surface of the sample altered at 70°C and pH 3 for 67. The reference one of quartz, cristobalite α and hydroxylapatite (XRD) are presented.

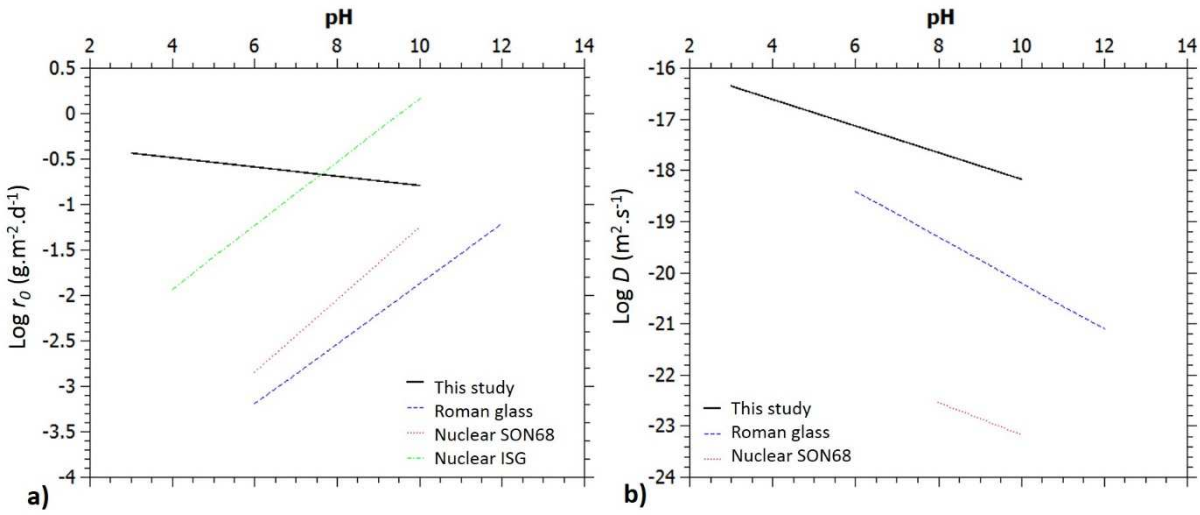

Figure 11. Theoretical evolution of dissolution and interdiffusion rate as a function of pH for different glass compositions. a) Logarithm of the initial dissolution rate r_0 according to the rate laws of this study (medieval-model type glass), Advocat et al., 1990 (SON68 nuclear glass), Inagaki et al., 2013 (ISG nuclear glass) and Verney-Carron et al., 2010 (Roman glass). Calculations were carried out at 25°C. b) Logarithm of the diffusion of K (this study), Na (Verney-Carron et al., 2010) (Roman glass) and B (Chave et al., 2007) (SON68 nuclear glass). Calculations were carried out at 30°C.

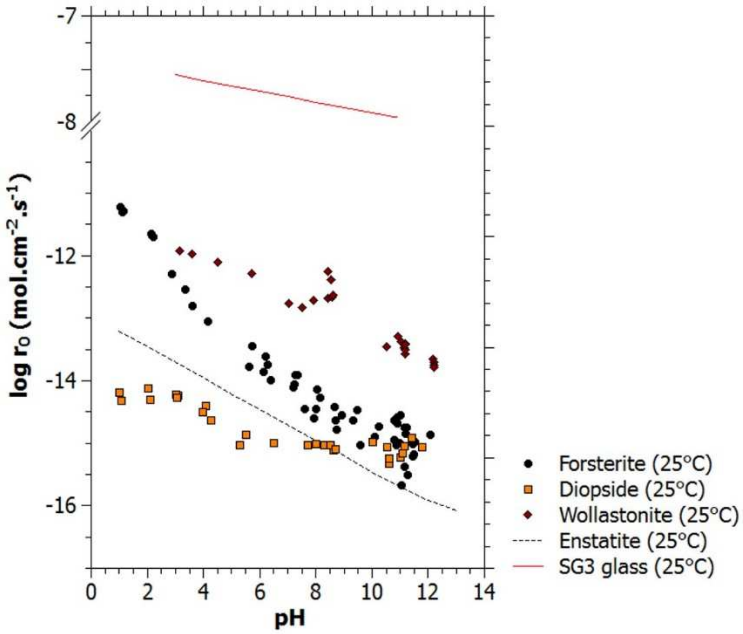

Figure 12. Logarithm of dissolution rate of several basic minerals in comparison with SG3 glass dissolution. Forsterite data (circles) come from Pokrovsky and Schott, 2000. Diopside and wollastonite (squares and diamonds, respectively) data come from Golubev et al., 2005. Enstatite data (dashed line) corresponds to predicted values from Oelkers and Schott, 2001. SG3 data corresponds to the predicted values calculated with the dissolution rate law (Eq. 9).

Table 1. Chemical composition (in wt.%) of SG3 model glass. Theoretical composition was calculated from the average of medieval glass analyses published in the literature and the actual composition of SG3 from 10 analyses performed by SEM-EDS.

	Oxides (wt. %)									
	SiO_2	Al_2O_3	K_2O	CaO	MgO	MnO	Na_2O	Fe_2O_3	P_2O_5	TiO_2
Theoretical composition	50.5	1.6	18.5	17.0	4.2	1.1	1.2	1.1	3.6	0.2
	± 4.4	± 0.7	± 3.8	± 3.9	± 1.9	± 0.5	± 0.7	± 0.6	± 1.5	± 0.1
Actual composition of SG3	51.3	1.8	19.2	16.8	4.0	1.0	1.1	1.2	3.8	0.0
	± 0.1	± 0.0	± 0.1	± 0.1	± 0.1	± 0.0	± 0.1	± 0.1	± 0.1	± 0.0

Table 2. Measured and simulated pH at several temperatures and alteration times. Underlined times correspond to linear Si release over time. Value of pH containing the (a) mention corresponds to a reactor that cracked during the experiment; the unmatched measured/simulated pH is due to the carbonation.

T (°C)	4						4				20									20						20			
t (d)	0	13.0	19.0	33.0	64.0	87.0	0.0	13.0	33.0	87.0	0	1.0	1.3	5.2	25.2	39.0	69.0	71.0	74.0	0.0	1.0	1.3	4.0	5.2	74.0	0.0	1.0	39.0	74.0
Measured pH at T_{amb}	4.8	7.2				6.5	9.9	10.0		10.1	3.0			2.4					7.3	6.2					8.0	10.0			10.2
Simulated pH at T_{exp}		6.3	6.5	6.9	7.3	7.3		9.9	10.3	10.8		2.9	3.0		3.5	3.7	4.0	4.2	7.3		6.3	6.7	6.8	7.0	7.7		10.0	9.9	10.1

T (°C)	35				35					35			50				50		50				50				50			
t (d)	0	1.0	9.0	26.0	0	1.0	5.0	8.0	26.0	0	1.0	21.0	0	1.0	4.0	24.0	0	24.0	0	1.0	4.0	24.0	0	1.0	4.0	24.0	0	1.0	5.0	24.0
Measured pH at T_{amb}	2.9			7.2	6.2				7.2	10.3		10.1	2.0			2.1	2.8	3.0	4.8			7.9	6.2			-	8.8			8.58
Simulated pH at T_{exp}		3.2	3.7	7.6		6.9	7.1	7.4	7.8		9.9	10.1	2.0	2.0	2.0	2.0	3.0	3.1	5.0	5.2	5.0	6.6		6.1	6.0	6.8	7.9	7.9	7.7	7.7

T (°C)	50				70						70								70						
t (d)	0	1.0	5.0	24.0	0	0.13	1.0	4.0	8.3	74.0	0	0.04	0.13	0.17	1.0	4.0	8.3	67.0	0	0.04	0.17	1.00	8.29	69.0	74.0
Measured pH at T_{amb}	9.7			9.9	3.0					8.8	6.2							5.45(a)	10.0						9.6
Simulated pH at T_{exp}	8.8	8.8	8.8	8.8		3.1	3.3	3.4	3.5	9.1	6.0	6.2	6.5	6.8	7.4	7.9	8.2	9.0	8.6	8.6	8.6	8.6	8.3	7.7	7.7

Table 3. Simulated pH at different temperatures and alteration times for the experiment in initially Si enriched solution.

T (°C)	20				70				70		
t (d)	0	6	20	83	0	6	20	83	0	6.0	64.0
Simulated pH at T_{exp}	8.3	10.2	10.3	11.3	9.0	9.6	9.8	9.8	10.5	10.4	10.4

Table 4. Initial dissolution rate r_0 at several pH and temperatures. Deviation (in %) between experimental values (r_0_exp) and theoretical values (r_0_model) was calculated.

T (K)	pH	r_0_exp	r_0_model	relative deviation
4	6.86	0.06	0.07	11%
4	10.04	0.03	0.04	33%
20	3.00	0.14	0.28	49%
20	6.70	0.11	0.18	36%
20	10.05	0.06	0.11	48%
35	3.00	0.68	0.63	8%
35	7.13	0.41	0.37	11%
35	10.00	0.26	0.25	0%
50	2.00	0.93	1.47	37%
50	3.00	0.94	1.29	27%
50	5.45	0.80	0.94	15%
50	6.30	0.77	0.84	8%
50	8.80	0.55	0.61	10%
70	3.26	3.56	2.95	21%
70	6.50	1.84	1.94	5%
70	8.57	1.47	1.49	1%

Table 5. Values of n and k_0 coefficients (k_0 in $g.m^{-2}.d^{-1}$) as a function of the temperatures T (in °C).

T	***n***	***k_0***
4	0.095	0.17
20	0.054 ± 0.015	0.22 ± 0.04
35	0.060 ± 0.005	1.05 ± 1.71
50	0.033 ± 0.006	1.16 ± 0.65
70	0.074 ± 0.011	6.00 ± 0.54

Table 6. Activation energies (in kJ.mol^{-1}) of glass dissolution at pH 3, 5, 6 and 10.

pH	***Ea***
3	50.5 ± 7.4
6	42.7 ± 3.0
8	45.3
10	48.4 ± 12.3

Table 7. Potassium diffusion coefficients (D_K in $m^2.s^{-1}$) as a function of pH and temperature (in °C). Values "DK_exp" correspond to the experimental data and were used for the adjustment of the interdiffusion rate law using Matlab software. "D_K_model" is the theoretical K diffusion coefficient calculated with the rate law.

T (°C)	pH	D_K_exp	D_K_model	Relative deviation (%)
22	3.0	3.20E-17	3.10E-17	3%
22	10.2	1.20E-18	4.16E-19	65%
20	11.0	2.50E-19	2.34E-19	6%
35	3.0	9.00E-17	5.61E-17	38%
50	3.0	1.00E-16	1.05E-16	5%
70	3.3	2.30E-16	1.90E-16	17%
70	9.7	7.00E-18	4.02E-18	43%
70	10.3	3.00E-18	2.80E-18	7%
50	2.0	1.80E-16	1.91E-16	6%

Table 8. Alteration thickness (e in µm) of samples altered at several pH and temperatures. Two thicknesses measured using SEM are indicated: the average thickness of the gel and the total thickness of the alteration layer, including secondary phases. The "/" sign indicates that the total thickness is equal to the gel thickness. Also, two thicknesses calculated using K, Ca and Si concentrations in solution are presented. NL_K-NL_{Si} and NL_{Ca}-NL_{Si} were divided by the density of the glass to obtain the thickness. For samples altered at pH > 9, no alteration layer was observed using SEM and regarding the limitations of the machine, the indicated thickness is < 0.1 µm. No %deviation was calculate for these concerned samples.

		SEM (gel)	SEM (total)	NL_K-NL_{Si}	NL_{Ca}-NL_{Si}	NL_K-NL_{Si}	NL_{Ca}-NL_{Si}
T (°C)	pH	e (µm)	e (µm)	e (µm)	e (µm)	% deviation	% deviation
4	6.9	0.7	/	2.0	0.2	190%	73%
4	10.0	<0.1	/	1.3	0.7	-	-
20	3.0	2.5	/	1.4	2.6	43%	4%
20	6.7	1.0	/	0.2	0.5	82%	52%
20	10.0	<0.1	/	0.3	0.0	-	-
70	3.3	6.8	61.7	5.1	0.0	25%	100%
70	6.5	30.0	95.4	50.0	33.6	67%	12%
70	8.9	<0.1	/	5.1	0.0	-	-

Table 9. Average composition (in wt. %) of the alteration layers of glass altered at 20 and 70°C at different pH values.

	wt. %	Na_2O	MgO	Al_2O_3	SiO_2	P_2O_5	K_2O	CaO	MnO	Fe_2O_3
20°C - pH 3	μ	0.3	1.0	10.9	**72.1**	1.6	**2.4**	**6.0**	1.0	4.8
	σ	0.1	0.3	0.4	0.4	0.7	1.0	0.4	0.1	1.2
20°C - pH 6	μ	0.6	2.4	9.9	**61.1**	2.4	**8.2**	**9.7**	1.1	4.6
	σ	0.1	0.2	0.1	1.4	0.1	1.0	1.0	0.2	3.6
70°C - pH 3	μ	0.2	5.1	6.5	**64.5**	3.5	**4.3**	**10.8**	2.0	3.1
	σ	0.2	6.3	2.1	4.6	3.0	4.6	4.5	1.4	0.6
70°C - pH 6	μ	0.1	2.3	7.0	**74.7**	4.8	**1.9**	**4.5**	1.3	3.5
	σ	0.1	4.2	3.0	8.3	3.2	0.5	1.8	0.7	1.2

Table 10. Saturation index of different phases calculated by the JCHESS software. Values in bold correspond to IS > 0 (supersaturation of the solution in relation to the phase considered). SiO_2(am) corresponds to the amorphous silica.

	20pH3	70pH3	70pH6	70pH8.5
time	67 d	67 d	67 d	39 d
Hydroxylapatite	**2.80**	**7.69**	**16.3**	-
Calcite	**-**	**0.50**	**2.27**	**1.0**
Quartz	**0.96**	**0.48**	**0.82**	**0.09**
Tridymite	**0.76**	**0.32**	**0.67**	-0.06
Chalcedony	**0.66**	**0.25**	**0.59**	-0.14
Cristobalite α	**0.37**	**0.02**	**0.36**	-0.37
Coesite	**0.11**	-0.23	**0.11**	-0.61
Cristobalite β	-0.08	-0.32	**0.02**	-0.71
SiO_2(am)	-0.38	-0.53	-0.19	-0.92

	Publication	This study	Verney-Carron et al., 2010	Chave et al., 2007	Advocat et al., 1990	Inagaki et al., 2013	Guy and Schott, 1989	Gislason and Oelkers, 2003
	Glass type	SG3 model	model	nuclear	nuclear	nuclear	basaltic	basaltic
		Stained glass	Roman	SON68	SON68	ISG		
	First major éléments (wt. %)	51% SiO_2	70% SiO_2	45% SiO_2	45% SiO_2	56% SiO_2	54% SiO2	48% SiO_2
		19% K_2O	19% Na_2O	14%B_2O_3	14%B_2O_3	17% B_2O_3	14 %MgO	14 %Al_2O_3
		17% CaO	5% CaO	10%Na_2O	10%Na_2O	12% Na_2O	13 % CaO	12% CaO
	pH range	3 à 10	6 à 12	8 à 10	6 à 10	4 à 10	1 à 11	1 à 11
	T range	5 à 70°C	15 à 90°C	30 à 90°C	25 à 100°C	25 à 90°C	50 à 200°C	6 à 300°C
Dissolution	*n*	0.056	-0.33	-	-0.4	-0.35	-0.72 à 50°C -0.06 à 200°C	0.33 (pour $(a^3(H^{+})/a(Al^{3+}))$
	k_0	5.0×10^6	5.79×10^9	-	1.20×10^8	8.70×10^8	-	6.08×10^4
	Ea	39.7	85.2	-	-	70	59	25.5
	Siliceous phase	SiO_2(am)	Cristobalite β	-	-	-	-	-
Interdiffusion	*n*	0.25	0.45	-0.32 (for $[OH^-]$)	-	-	-	-
	D_0	2.40×10^{-10}	7.30×10^{-3}	2.21×10^{-11}	-	-	-	-
	Ea	34.5	78.7	85.3	-	-	-	-

Table 11. Dissolution and interdiffusion rate parameters for Advocat et al., 1990; Chave et al., 2007; Gislason and Oelkers, 2003; Guy and Schott, 1989; Inagaki et al., 2013; Verney-Carron et al., 2010 on different types of glasses. Parameters of Inagaki et al. (2013) were determined from the data. T is the temperature (in °C), *n* is the pH dependence coefficient, *Ea* is the activation energy (in $kJ.mol^{-1}$), k_0 is the kinetic constant (in $g.m^{-2}.d^{-1}$) and D_0 is the diffusion constant (in $m^2.s^{-1}$). For Chave et al. (2007), *n* parameter is relative to OH^- concentration and not H^+. For Guy and Schott, 1989, *n* parameter depends of T. For Gislason and Oelkers (2003), the pH-dependence is related to the ratio of H^+ and Al^{3+} activities.